Lipid droplets control mitogenic lipid mediator production in human cancer cells

Eva Jarc Jovičić[1,2], Anja Pucer Janež[1,2], Thomas O. Eichmann[3,4], Špela Koren[1,2], Vesna Brglez[1,2], Paul M. Jordan[5], Jana Gerstmeier[5], Duško Lainšček[6,7], Anja Golob-Urbanc[6], Roman Jerala[6,7], Gérard Lambeau[8], Oliver Werz[5], Robert Zimmermann[3,9], and Toni Petan[1,*]

[1]Department of Molecular and Biomedical Sciences, Jožef Stefan Institute, Ljubljana, Slovenia
[2]Jožef Stefan International Postgraduate School, Ljubljana, Slovenia
[3]Institute of Molecular Biosciences, University of Graz, Graz, Austria
[4]Center for Explorative Lipidomics, BioTechMed-Graz, Graz, Austria
[5]Department of Pharmaceutical/Medicinal Chemistry, Institute of Pharmacy, Friedrich Schiller University Jena, Jena, Germany
[6]Department of Synthetic Biology and Immunology, National Institute of Chemistry, Ljubljana, Slovenia
[7]EN-FIST, Centre of Excellence, Ljubljana, Slovenia
[8]Université Côte d'Azur (UCA), Centre National de la Recherche Scientifique (CNRS), Institut de Pharmacologie Moléculaire et Cellulaire (IPMC), UMR7275, Valbonne Sophia Antipolis, France
[9]BioTechMed-Graz, University of Graz, Graz, Austria

Running title: Lipid droplets and lipid mediators

*To whom correspondence should be addressed:
Toni Petan
Department of Molecular and Biomedical Sciences
Jožef Stefan Institute
Jamova cesta 39
SI-1000 Ljubljana
Slovenia
Tel: +386-1-4773713
Fax: +386-1-4773984
E-mail: toni.petan@ijs.si

Abstract

Polyunsaturated fatty acids (PUFAs) are components of membrane phospholipids and precursors of bioactive lipid mediators. Here, we investigated the crosstalk of three pathways providing PUFAs for lipid mediator production: (i) secreted group X phospholipase A_2 (GX $sPLA_2$) and (ii) cytosolic group IVA PLA_2 ($cPLA_2\alpha$), which both mobilize PUFAs from phospholipids, and (iii) adipose triglyceride lipase (ATGL), which breaks down triacylglycerols (TAGs) stored in lipid droplets (LDs). Combining lipidomic and functional analyses, we demonstrate that lipid mediator production depends on TAG turnover. GX $sPLA_2$ directs PUFAs into TAGs and ATGL is required for their entry into lipid mediator biosynthetic pathways. ATGL also promotes the incorporation of LD-derived PUFAs into phospholipids representing substrates for $cPLA_2\alpha$. Additionally, inhibition of TAG synthesis mediated by acyl-CoA:diacylglycerol acyltransferase 1 (DGAT1) reduces the levels of mitogenic lipid signals and compromises tumour growth. This study expands the paradigm of PLA_2-driven lipid mediator signalling and identifies LDs as central lipid mediator production hubs.

Keywords: lipid droplets, diacylglycerol acyltransferase, adipose triglyceride lipase, phospholipase A_2, lipid mediators, cancer

63 # Introduction

64

65 Fatty acids (FAs) are universal cellular energy sources and membrane building blocks.
66 FAs are also involved in signalling pathways that control cell growth, inflammation and
67 tumourigenesis (Röhrig & Schulze, 2016). The ensemble of signalling FAs is vastly expanded
68 by the oxygenation of polyunsaturated FAs (PUFAs) by cyclooxygenase (COX), lipoxygenase
69 (LOXs) and CYP450 monooxygenase enzymes into several families of bioactive lipid
70 mediators, including the eicosanoids (Dennis & Norris, 2015). These short-lived autocrine and
71 paracrine signalling molecules are released from cells to collectively modulate various
72 processes in their microenvironment, e.g., to orchestrate a shift into pro-inflammatory or anti-
73 inflammatory states. Pathways that control the availability of different PUFAs for oxygenation
74 determine the types of lipid mediator species produced and the dynamics of their production
75 (Wang & DuBois, 2010; Greene *et al*, 2011). Our current understanding of the control of PUFA
76 supply for lipid mediator production is limited, particularly as this is intrinsically dependent on
77 complex (PU)FA metabolism, including PUFA biosynthesis, uptake, storage, breakdown, lipid
78 remodelling and trafficking (Pérez-Chacón *et al*, 2009; Astudillo *et al*, 2019; Jarc & Petan,
79 2020).

80 The canonical pathway that supplies arachidonic acid (AA) for eicosanoid production
81 depends on the group IVA cytosolic phospholipase A_2 (cPLA$_2$α), whose role in stimulus-
82 induced eicosanoid production has been demonstrated in various pathophysiological settings
83 (Bonventre *et al*, 2004; Shimizu, 2009; Murakami *et al*, 2011; Leslie, 2015). Upon cell
84 activation, cPLA$_2$α binds to perinuclear membranes of the ER and Golgi complex and
85 selectively hydrolyses phospholipids containing AA at the *sn*-2 position (Hayashi *et al*, 2021).
86 Numerous other members of the PLA$_2$ superfamily promote lipid mediator production, either
87 through activation of cPLA$_2$α or by acting independently on their respective phospholipid pools,
88 thereby releasing not only AA but also other PUFAs (Saiga *et al*, 2005; Duchez *et al*, 2019;
89 Astudillo *et al*, 2019). In particular, several secreted PLA$_2$s (sPLA$_2$s) have been implicated in
90 lipid mediator production (Murase *et al*, 2016; Sato *et al*, 2020). The group X sPLA$_2$ is the most
91 potent among mammalian sPLA$_2$s at hydrolysing the phosphatidylcholine (PC)-rich plasma
92 membrane, lipoproteins and extracellular vesicles (Bezzine *et al*, 2002; Mounier *et al*, 2004;
93 Jarc *et al*, 2018; Kudo *et al*, 2022). It releases various unsaturated FAs, including ω-3 and ω-
94 6 PUFAs, and it is involved in inflammation, immunity and cancer (Surrel *et al*, 2009; Murase
95 *et al*, 2016; Schewe *et al*, 2016; Pucer *et al*, 2013; Ogden *et al*, 2020; Kudo *et al*, 2022).

96 Recent studies suggest that besides membrane phospholipids, other cellular lipid
97 pools, including neutral lipids stored in lipid droplets (LDs) or derived from lipoprotein uptake,
98 are also sources of PUFAs for lipid mediator production (Dichlberger *et al*, 2014; Schlager *et*

99 *al*, 2015, 2017; Jarc & Petan, 2020). LDs are specialized organelles that store FAs and other
100 lipids in their esterified forms, primarily as triglycerides (TAGs) and sterol esters (Welte &
101 Gould, 2017; Olzmann & Carvalho, 2019). A hallmark role of LDs is taking up excess FAs to
102 prevent lipotoxicity and fine-tune FA release via lipolysis to match various cellular demands
103 (Listenberger *et al*, 2003; Rambold *et al*, 2015; Nguyen *et al*, 2017; Henne *et al*, 2018; Petan,
104 2020). Adipose triglyceride lipase (ATGL), the major mammalian TAG lipase, provides FAs for
105 mitochondrial energy production, but it also controls FA-induced signalling pathways that
106 coordinate metabolism and inflammation (Zimmermann *et al*, 2004; Haemmerle *et al*, 2011;
107 Schweiger *et al*, 2017; Zechner *et al*, 2017). In immune and cancer cells, LDs have long been
108 implicated in AA storage, trafficking and eicosanoid production (Dvorak *et al*, 1983; Triggiani
109 *et al*, 1994; Bozza *et al*, 2011). It was only recently shown that ATGL provides precursors for
110 lipid mediator production and modulates neutrophil immune responses *in vivo* (Dichlberger *et*
111 *al*, 2014; Schlager *et al*, 2015; Riederer *et al*, 2017). However, it is not yet clear how LDs
112 manage PUFA trafficking for lipid mediator production in mammalian cells and how they
113 cooperate with the canonical PLA_2-mediated pathways (Guijas *et al*, 2014; Jarc & Petan,
114 2020).

115 The trafficking of PUFAs between membranes and LDs is an emerging mechanism
116 controlling PUFA oxygenation and lipid-induced oxidative damage, including ferroptotic cell
117 death. On the one hand, the sequestration of PUFAs into LDs limits their availability for
118 oxidation (Bailey *et al*, 2015; Jarc *et al*, 2018; Dierge *et al*, 2021). For instance, in fly embryos
119 exposed to hypoxia, membrane lipid peroxidation and neuronal damage are prevented via a
120 mechanism mediated by phospholipase D and diacylglycerol acyltransferase (DGAT) that
121 diverts PUFAs from phospholipids into TAGs stored within LDs (Bailey *et al*, 2015). On the
122 other hand, the proportion of (poly)unsaturated FAs released from LDs may determine
123 membrane saturation, oxidative stress and cell fate (Ackerman *et al*, 2018; Jarc *et al*, 2018).
124 Accordingly, in cancer cells exposed to exogenous PUFAs, LDs are enriched with PUFA-TAGs
125 and their hydrolysis by ATGL promotes oxidative stress-dependent cell death (Jarc *et al*,
126 2018). Under these conditions, the transfer of unsaturated FAs from membrane phospholipids
127 into LDs mediated by the human group X (hGX) $sPLA_2$ balances phospholipid and TAG acyl-
128 chain composition and prevents PUFA lipotoxicity (Pucer et al, 2013; Jarc *et al*, 2018). Based
129 on these findings, we hypothesize that LD turnover modulates membrane PUFA content and
130 affects PLA_2-mediated lipid mediator production.

131 Here, we investigated the crosstalk between different molecular pathways providing
132 PUFAs for lipid mediator production in human cancer cells. We show that the incorporation of
133 PUFAs into TAGs and their subsequent release via lipolysis are essential for production of
134 mitogenic lipid mediators. We demonstrate that LDs integrate several PUFA trafficking
135 pathways and act as central hubs that control PLA_2-driven lipid mediator production.

136 Furthermore, we provide evidence for a pathophysiological relevance of these findings by
137 showing that inhibition of TAG synthesis impairs the production of mitogenic lipid mediators
138 and reduces cancer cell proliferation in vitro and tumour growth in vivo.
139
140
141 # Results
142
143 ***Membrane phospholipid hydrolysis by hGX sPLA$_2$ leads to enrichment of LDs with long-***
144 ***chain PUFA-TAGs***
145 We have shown previously that hGX sPLA$_2$ releases various unsaturated FAs from adherent
146 cells, including oleic acid (C18:1n–9; OA) and PUFAs (Jarc *et al*, 2018), and induces LD
147 accumulation in several breast cancer cell lines (Pucer *et al*, 2013; Jarc *et al*, 2018).
148 Recombinant hGX sPLA$_2$ also induced LD accumulation in other cancer and immortalised non-
149 tumorigenic cell lines (Fig. 1A, B), suggesting that its effects on LD metabolism are not limited
150 to specific cell types. Here we asked whether hGX sPLA$_2$ alters TAG acyl chain composition
151 in LDs of MDA-MB-231 cells (Fig. 1C), a cell line showing enhanced proliferation and
152 resistance to starvation upon treatment with hGX sPLA$_2$ (Pucer *et al*, 2013). Cells pre-
153 incubated with [^{14}C]-OA readily incorporated the radiolabelled FA into phospholipids and
154 TAGs, while hGX sPLA$_2$ treatment specifically increased the abundance of TAGs containing
155 [^{14}C]-OA in various growth conditions (Fig. 1D; Supp. Fig. 1A, B). Lipidomic LC/MS analyses
156 of TAG species extracted from hGX sPLA$_2$-treated serum-fed (Fig. 1E–H, J, K; Supp. Fig. 1C,
157 D) and serum-starved cells (Fig. 1F, I) revealed an unexpected enrichment of TAG species
158 with long-chain (Fig. 1J) and highly unsaturated FAs (Fig. 1K). This suggests that among the
159 unsaturated FAs released by hGX sPLA$_2$, the polyunsaturated species are preferentially
160 redistributed from membrane phospholipids into LDs. Experiments with serum-starved cells
161 (Fig. 1D, F, I) demonstrated that serum lipoproteins, which are major targets for the enzyme
162 (Guillaume *et al*, 2015; Jarc *et al*, 2018), are not required for hGX sPLA$_2$-induced enrichment
163 of TAGs with PUFAs. This observation suggests a direct action of hGX sPLA$_2$ on the plasma
164 membrane leading to enrichment of LDs with PUFA-containing TAGs.
165
166 ***ATGL-mediated LD breakdown is required for PGE$_2$ production in serum-starved cells***
167 Serum withdrawal induces LD breakdown in most cell types (Bosch *et al*, 2020). Given the
168 hGX-sPLA$_2$-induced enrichment of LDs with PUFAs, we next asked if starvation-induced
169 breakdown of PUFA-rich LDs is sufficient to stimulate eicosanoid production. LD biogenesis
170 was first stimulated with hGX sPLA$_2$ (or with exogenous AA) in cells grown in serum-rich
171 medium. Then the cells were serum-starved in the absence of these stimuli to induce LD

172 breakdown (Fig. 2A; Supp. Fig. 2A). In comparison with untreated cells, the serum-starved
173 cells pre-treated with hGX $sPLA_2$ released more glycerol (Supp. Fig. 2C), an indicator of TAG
174 lipolysis, and produced more prostaglandin (PG)E_2 (Fig. 2B), a major AA-derived eicosanoid.
175 Although HeLa cells were unique among cell lines in showing a net reduction in neutral lipid
176 levels upon treatment with hGX $sPLA_2$ (Fig. 1A, B; Supp. Fig. 2B), there was an increase in
177 lipolysis (Supp. Fig. 2C) and PGE_2 production (Fig. 2B) during serum starvation. This is
178 indicative of an accelerated LD turnover in hGX-$sPLA_2$-treated HeLa cells that leads to net
179 reduction in LD levels and drives lipid mediator production. Similarly, pre-treatment with
180 exogenous AA led to increased PGE_2 production in starving MDA-MB-231 and HeLa cells
181 (Supp. Fig. 2D). These observations indicate that LD breakdown drives PGE_2 synthesis.
182 We next investigated if ATGL, the rate-limiting enzyme in intracellular TAG lipolysis, is
183 responsible for LD breakdown and PGE_2 biosynthesis observed during starvation. ATGL
184 silencing using siRNA in MDA-MB-231 and HeLa cells (Fig. 2C; Supp. Fig. 2E) reduced
185 glycerol release (Supp. Fig. 2F, G), increased LD abundance (Fig. 2D, F; Supp. Fig. 2H, J)
186 and reduced basal and hGX-$sPLA_2$-induced PGE_2 production during serum starvation (Fig. 2E;
187 Supp. Fig. 2I). ATGL deficiency also attenuated LD breakdown and suppressed the production
188 of PGE_2 in MDA-MB-231 cells pre-treated with exogenous AA (Supp. Fig. 2N, O). However,
189 although ATGL knockdown increased LD abundance also in A549 cells (Supp. Fig. 2E; Supp.
190 Fig. 2K, M), it unexpectedly augmented glycerol release (Supp. Fig. 2F, G) and failed to
191 suppress basal or hGX-$sPLA_2$-induced PGE_2 production (Supp. Fig. 2L). In contrast to the
192 effects of ATGL silencing, ATGL overexpression in the breast and cervical cancer cells (Fig.
193 2G; Supp. Fig. 2P) stimulated glycerol release (Fig. 2H) and enhanced PGE_2 production (Fig.
194 2I), albeit without significantly altering neutral lipid levels (Supp. Fig. 2R). The effects of ATGL
195 overexpression were fully reversed in the presence of ATGL-targeting siRNA (Fig. 2H, I).
196 Collectively, these data demonstrate that LD breakdown via ATGL is required for basal, AA-
197 induced and hGX-$sPLA_2$-stimulated PGE_2 production (Fig. 2J) in MDA-MB-231 and HeLa cells,
198 but not in the A549 cells.
199
200 ***ATGL-mediated release of ω-3 and ω-6 PUFAs from LDs drives lipid mediator***
201 ***production***
202 The data presented above demonstrate that transient storage of AA within LD TAGs followed
203 by AA release from TAGs by ATGL are intermediate steps in basal and hGX-$sPLA_2$-stimulated
204 production of PGE_2. To find out if ATGL-mediated TAG lipolysis promotes the production of a
205 wider range of eicosanoids and related lipid mediators (which might also derive from other
206 PUFAs), we performed targeted liquid chromatography-tandem mass spectrometry-based
207 metabololipidomics to examine the effects of ATGL silencing on the lipid mediator profiles of
208 untreated and hGX-$sPLA_2$-treated cells. Here, pre-treatment of breast cancer cells with hGX

209 $sPLA_2$ stimulated the starvation-induced production of numerous lipid mediators,
210 biosynthesised from different PUFAs by various enzymatic pathways (Fig. 3A–C, Supp. Fig.
211 3). hGX $sPLA_2$ promoted the synthesis of eicosapentaenoic acid (EPA)-derived lipid mediators,
212 as well as the production of AA-derived and DHA-derived products. ATGL depletion
213 suppressed the release of all of the hGX-$sPLA_2$-induced lipid mediators (Fig. 3A–C, Supp. Fig.
214 3). Furthermore, ATGL silencing strongly inhibited the basal, hGX-$sPLA_2$-independent
215 production of lipid mediators, including PGE_2. Starving cells pre-treated with hGX $sPLA_2$ also
216 released more unesterified PUFAs, including AA, EPA and DHA, which was prevented by
217 ATGL silencing (Fig. 3D). This suggested that a portion of hGX $sPLA_2$-released PUFAs is not
218 used for lipid mediator production or incorporated into membranes, but is rather released from
219 cells through lipolysis by ATGL. Overall, these observations suggest that ATGL controls the
220 availability of PUFAs for lipid mediator synthesis (Fig. 3E).
221
222 ***Inhibition of DGAT-mediated LD biogenesis impairs PGE_2 production***
223 To examine whether the incorporation of PUFAs into TAGs is a prerequisite for the conversion
224 of PUFAs into lipid mediators, we inhibited TAG synthesis using a combination of specific
225 inhibitors of DGAT1 and DGAT2 (DGATi), which mediate the final committed step in TAG
226 synthesis, and followed changes in LD turnover and lipid mediator production. Combined
227 inhibition of both DGATs was necessary because individual inhibition of DGAT1 or DGAT2 did
228 not reduce neutral lipid levels in hGX-$sPLA_2$-treated cells (Supp. Fig. 4A). Combined DGAT1
229 and DGAT2 inhibition during serum feeding strongly suppressed basal, hGX-$sPLA_2$-induced
230 and exogenous AA-induced LD accumulation (Fig. 4A, B, D). There was an almost complete
231 depletion of LDs in serum-fed DGATi-treated cells (Fig. 4B), which allowed only a minimal
232 breakdown of residual LDs during the subsequent serum starvation (Fig. 4A). Notably, cells
233 depleted of LDs displayed low basal PGE_2 release and did not increase PGE_2 production upon
234 stimulation with either hGX $sPLA_2$ or exogenous AA (Fig. 4C, E). These results were
235 corroborated by lipidomic analyses, which showed that combined inhibition of DGAT1 and
236 DGAT2 suppresses hGX $sPLA_2$-induced production of several AA- and EPA-derived lipid
237 mediators (Fig. 4F; Supp. Fig. 4B), reduces exogenous AA-induced production of
238 prostaglandins (Supp. Fig. 4C) and blunts the release of unesterified PUFAs from starving
239 MDA-MB-231 cells (Fig. 4G). Notably, DGATi treatment abolished PGE_2 production also in
240 A549 cells (Fig. 4C), whereas ATGL depletion failed to do so (Supp. Fig. 2L), suggesting that
241 TAG synthesis precedes eicosanoid production in these cells as well. Therefore, DGAT-
242 mediated TAG biosynthesis under serum-rich conditions is a prerequisite for lipid mediator
243 production in serum-starved cells.
244 Besides promoting LD breakdown, serum removal in MDA-MB-231 cells stimulates the
245 transcription of lipogenic genes, including the sterol-regulatory element binding 1 protein

246 (SREBP-1) transcription factor and key enzymes involved in FA synthesis (Pucer *et al*, 2013).
247 In accordance with ongoing lipogenesis, treatment of serum-starved cells with hGX $sPLA_2$
248 resulted in a net increase in TAG levels (Fig. 1F). To examine whether TAG synthesis occurring
249 during serum starvation regulates eicosanoid production, control and ATGL-depleted cells
250 were treated with DGAT1 and DGAT2 inhibitors during serum feeding or during serum
251 starvation. As expected, DGAT inhibition during serum feeding fully depleted MDA-MB-231
252 and HeLa cells of LDs, thereby abolishing the effects of hGX $sPLA_2$ and ATGL silencing on LD
253 abundance (Supp. Fig. 4D). In contrast, DGAT inhibition during serum starvation did not affect
254 LD abundance in these two cell lines (Fig. 4H; Supp. Fig. 4E), nor did it affect PGE_2 release in
255 MDA-MB-231 cells (Fig. 4H). However, DGAT inhibition in serum-starved A549 cells reduced
256 LD abundance and suppressed PGE_2 production (Fig. 4I). This was observed in both control
257 and in ATGL-deficient A549 cells indicating that the build-up of TAG stores during starvation
258 drives eicosanoid biosynthesis via an ATGL-independent mechanism. Accordingly, DGAT
259 inhibition during both serum feeding and starvation was necessary for full suppression of PGE_2
260 production in A549 cells (Supp. Fig. 4F).
261 Collectively, these results demonstrate that DGAT-mediated TAG synthesis and LD
262 turnover are required for lipid mediator production. ATGL-mediated breakdown of pre-existing
263 DGAT-induced LDs is the predominant mechanism of LD-driven eicosanoid production in the
264 serum-starved MDA-MB-231 breast and HeLa cervical cancer cells. On the contrary, A549
265 lung cancer cells employ TAG synthesis during starvation and ATGL-independent
266 mechanisms to support eicosanoid production.
267
268 ***$cPLA_2\alpha$ cooperates with ATGL and depends on LD turnover to drive eicosanoid***
269 ***production***
270 Given the well-accepted role of $cPLA_2\alpha$ in providing AA for eicosanoid biosynthesis, we next
271 asked whether $cPLA_2\alpha$ participates in LD-driven lipid mediator production. We speculated that
272 at least three main scenarios are possible (Fig. 5A): (a) $cPLA_2\alpha$-induced incorporation of
273 phospholipid-derived AA into TAGs, followed by AA release from LDs by ATGL; (b) ATGL-
274 dependent transfer of TAG-derived AA into phospholipid pools, which are then accessed by
275 $cPLA_2\alpha$; and (c) a lipid-droplet-independent action of $cPLA_2\alpha$ on membrane phospholipids.
276 To examine these possibilities, we first used siRNA to deplete cells of $cPLA_2\alpha$ alone or
277 in combination with ATGL (Fig. 5B; Supp. Fig. 5A, B). $cPLA_2\alpha$ deficient cancer cells had slightly
278 increased neutral lipid levels (Fig. 5B; Supp. Fig. 5C), but contained a significantly higher
279 number of LDs (Fig. 5C; Supp. Fig. 5E, F). This finding was particularly evident in ATGL-
280 deficient and hGX $sPLA_2$ pre-treated starving cells and suggests a modulatory role of $cPLA_2\alpha$
281 in LD turnover. In line with its major role in TAG lipolysis, the predominant effect of ATGL
282 silencing on LD morphology was an increase in LD diameters, along with some minor changes

283 in the number of LDs per cell (Fig. 5C; Supp. Fig. 5E, F). Most notably, $cPLA_2\alpha$ depletion in
284 A549 cells, but not ATGL silencing, abolished basal and hGX-$sPLA_2$-induced eicosanoid
285 release (Fig. 5B). On the contrary, while ATGL knockdown lowered PGE_2 production in MDA-
286 MB-231 cells, $cPLA_2\alpha$ silencing did not alter PGE_2 levels. Of note, the silencing of $cPLA_2\alpha$ in
287 HeLa cells led to a marked increase in PGE_2 release, which was partially reduced upon
288 depletion of both ATGL and $cPLA_2\alpha$ (Fig. 5B). These data suggested that $cPLA_2\alpha$ modulates
289 LD turnover and that its contribution to PGE_2 production during serum starvation is cell type-
290 specific.

291 To find out more about the interplay between $cPLA_2\alpha$ and ATGL, we asked how
292 reciprocal overexpression of one and silencing of the other might affect LD turnover and PGE_2
293 production (Fig. 5D). In all three cell lines, the overexpression of ATGL or $cPLA_2\alpha$ had a
294 minimal effect on neutral lipid levels (Supp. Fig. 5D, G, H), but both significantly augmented
295 PGE_2 production (Fig. 5D). ATGL silencing blocked PGE_2 production induced by
296 overexpression of $cPLA_2\alpha$ in MDA-MB-231 and HeLa cells, whereas $cPLA_2\alpha$ silencing only
297 partially reduced ATGL-overexpression-driven eicosanoid production in MDA-MB-231 cells,
298 and even increased it in HeLa cells. On the contrary, in A549 cells, ATGL knockdown did not
299 affect $cPLA_2\alpha$-induced PGE_2 production, but silencing of $cPLA_2\alpha$ reduced PGE_2 release from
300 ATGL-overexpressing cells (Fig. 5D). Taken together, these data suggested that ATGL is the
301 main enzyme in the provision of PUFAs for eicosanoid production in MDA-MB-231 and HeLa
302 cells, whereby $cPLA_2\alpha$ stimulation of eicosanoid production depends on ATGL. In contrast, in
303 A549 cells, $cPLA_2\alpha$ has a dominant role in PGE_2 production, which is independent of ATGL,
304 but is still associated with changes in LD turnover.

305 To examine if TAG synthesis is involved in $cPLA_2\alpha$-driven lipid mediator production,
306 $cPLA_2\alpha$ and ATGL were overexpressed in cells depleted of LDs using DGAT inhibitors (Fig.
307 5E; Supp. Fig. 5H). As expected, TAG synthesis was necessary for ATGL stimulation of
308 eicosanoid production (Fig. 5E). However, in all three cell lines, $cPLA_2\alpha$-overexpression-
309 induced eicosanoid production was also completely abolished upon DGAT inhibition (Fig. 5E).
310 Therefore, LDs are required for $cPLA_2\alpha$-driven lipid mediator production. $cPLA_2\alpha$ and ATGL
311 appear to have cell-type-specific roles that are either cooperative or complementary for both
312 LD turnover and eicosanoid production. In the breast and cervical cancer cells, deficiency of
313 ATGL impairs $cPLA_2\alpha$-induced PGE_2 production, which suggests the possibility that the
314 transfer of AA from TAGs to phospholipids is a prerequisite for the action of $cPLA_2\alpha$.

315

316 ***ATGL and $cPLA_2\alpha$ have complementary roles in TAG and phospholipid acyl-chain***
317 ***remodelling***

318 To examine how hGX $sPLA_2$, ATGL and $cPLA_2\alpha$ affect PUFA trafficking between the
319 phospholipid and TAG pools in MDA-MB-231 cells during serum starvation, we performed

320 single and double knockdowns of ATGL and $cPLA_2\alpha$ followed by lipidomic analyses comparing
321 the lipid compositions of cells first pre-treated with hGX $sPLA_2$ during nutrient sufficiency and
322 subsequently serum-starved for 0 h, 3 h or 24 h (Fig. 6A).

323 First, hGX $sPLA_2$ treatment led to enrichment of both TAGs and phospholipids with
324 PUFAs (Fig. 6A; Supp. Fig. 6A; Supp. Fig. 7A). hGX-$sPLA_2$-induced PUFA-TAG enrichment
325 was seen for serum-fed MDA-MB-231 cells, and it persisted upon hGX $sPLA_2$ and serum
326 withdrawal. Importantly, the levels of PUFA-containing phospholipids (PUFA-PLs)
327 progressively increased during the course of serum starvation (Supp. Fig. 6A). These data
328 suggest that a significant portion of $sPLA_2$-released PUFAs that are incorporated into TAGs in
329 serum-fed cells are gradually released via lipolysis during serum starvation and are re-
330 esterified into phospholipids.

331 Second, ATGL silencing led to an increased abundance of most TAG species, but also
332 altered phospholipid composition (Fig. 6A; Supp. Fig. 6A). The retention of various TAG
333 species within LDs due to ATGL deficiency is in agreement with the general lack of TAG acyl-
334 chain specificity of ATGL (Eichmann et al, 2012). During serum starvation, ATGL depletion
335 caused a gradual increase of numerous PUFA-TAGs (Fig. 6B), which confirmed that ATGL
336 hydrolyses PUFA-TAGs in starving cells. Importantly, ATGL deficiency reverted the elevation
337 of PUFA-PLs induced by hGX $sPLA_2$ pre-treatment (Supp. Fig. 6A). This is consistent with a
338 reduced flux of PUFAs from TAGs into phospholipids due to ATGL depletion. Thus, ATGL
339 hydrolyses various TAG species, including numerous PUFA-TAGs, and provides PUFAs for
340 esterification into phospholipids.

341 Third, depletion of $cPLA_2\alpha$ predominantly affected phospholipid (Fig. 6A; Supp. Fig.
342 6A), but also altered TAG composition (Fig. 6C). Numerous PUFA-PC and PUFA-
343 phosphatidylethanolamine (PUFA-PE) species were progressively elevated in $cPLA_2\alpha$-
344 deficient cells over the course of the serum starvation (Supp. Fig. 6A), which suggested that
345 these lipids are targeted by $cPLA_2\alpha$. The decreased abundance of PUFA-PLs observed in
346 ATGL-deficient cells was reversed in double-knockdown cells (Fig. 6A; Supp. Fig. 6B), which
347 suggested that ATGL-derived PUFAs are incorporated into a phospholipid pool that is targeted
348 by $cPLA_2\alpha$. A LION/web lipid ontology analysis suggested that the increased content of PUFA-
349 PLs in $cPLA_2\alpha$-deficient cells leads to significant changes in membrane biophysical properties,
350 including increased lateral diffusion, reduced bilayer thickness and a lower transition
351 temperature (Supp. Fig. 7B, C). Furthermore, $cPLA_2\alpha$ silencing did not affect hGX-$sPLA_2$-
352 induced PUFA-TAG enrichment (Fig. 6A), but it reduced the content of SFA/MUFA-TAGs (Fig.
353 6C). This effect was fully reversed in double-knockdown cells, suggesting that $cPLA_2\alpha$
354 depletion alters TAG composition in an ATGL-dependent manner. Therefore, ATGL promotes
355 the transfer of PUFAs from TAGs into a phospholipid pool that is targeted by $cPLA_2\alpha$, which in
356 turn reciprocally modulates the TAG pool.

357 Collectively, our results suggest that hGX-sPLA$_2$-liberated PUFAs are first and
358 predominantly incorporated into TAGs of growing LDs, and are then redistributed into
359 phospholipids upon TAG lipolysis by ATGL, particularly during serum starvation (Fig. 6D).
360 Some of the ATGL-released PUFAs are directly used for eicosanoid production (i.e.,
361 independent of cPLA$_2$α), while some are re-esterified into phospholipids and can be then
362 mobilised by cPLA$_2$α for the production of eicosanoids.
363
364 ***LDs drive cancer cell proliferation by promoting eicosanoid production***
365 Given that PGE$_2$ and other eicosanoids are mitogenic factors that promote tumour
366 growth (Wang & DuBois, 2010), we next asked whether LD turnover by DGAT and ATGL
367 affects cancer cell proliferation and possibly mediates the proliferative effect of hGX sPLA$_2$
368 (Surrel *et al*, 2009; Pucer *et al*, 2013). The induction of MDA-MB-231 cell proliferation by hGX
369 sPLA$_2$ was fully blocked by DGAT1 inhibition and by concurrent inhibition of both DGAT1 and
370 DGAT2; however, DGAT2 inhibition alone had no effects (Fig. 7A). Inhibition of DGAT1, but
371 not DGAT2, also reduced the basal, hGX-sPLA$_2$-independent rate of breast cancer cell
372 proliferation (Fig. 7A) and colony formation (Supp. Fig. 8A, B). As ATGL promotes lipid
373 mediator production, we hypothesized that ATGL overexpression should induce cell
374 proliferation in a COX/LOX-dependent manner. Indeed, alone or in combination with sPLA$_2$
375 treatment, ATGL overexpression stimulated cancer cell proliferation (Fig. 7B, C), which was
376 suppressed by the non-selective COX and LOX inhibitors indomethacin and
377 nordihydroguaiaretic acid, respectively (Fig. 7B, C). Exogenous PGE$_2$ stimulated MDA-MB-
378 231 cell proliferation, confirming its mitogenic potency under the present conditions (Supp. Fig.
379 8C). The effect of PGE$_2$ was suppressed by inhibition of DGAT1, but not by inhibition of
380 DGAT2, which suggested a positive-feedback loop between eicosanoids and DGAT1-
381 mediated TAG turnover. To examine the relevance of DGAT1-driven lipid mediator production
382 for cancer cell proliferation *in vivo*, we treated mice bearing aggressive MDA-MB-231
383 xenografts with DGAT1 inhibitors, followed tumour growth and determined lipid mediator
384 content in tumours. DGAT1 inhibitor treatments reduced tumour volume and prolonged the
385 survival of mice (Fig. 7D, E). Furthermore, tumour samples of DGAT1 inhibitor-treated mice
386 contained reduced levels of lipid mediators (Fig. 7F). Thus, DGAT1 inhibition supressed lipid
387 mediator production and tumour growth leading to prolonged survival of mice bearing breast
388 cancer xenografts. Altogether, these results with MDA-MB-231 cancer cells demonstrate that
389 DGAT1-mediated PUFA incorporation into LDs and PUFA release via ATGL drive basal and
390 hGX-sPLA$_2$-induced production of COX- and LOX-derived lipid mediators that in turn stimulate
391 cancer cell proliferation and tumour growth.
392 cPLA$_2$α-induced eicosanoid production promotes cancer cell proliferation and tumour
393 growth (Leslie, 2015; Koundouros *et al*, 2020), although this activity has not yet been

394 associated with LDs. As $cPLA_2\alpha$ has a major role in LD-dependent eicosanoid production in
395 A549 cells (Fig. 5B), we asked whether $cPLA_2\alpha$ stimulates A549 cell proliferation in a DGAT-
396 and COX-dependent manner. Indeed, $cPLA_2\alpha$-overexpression led to increased A549 cell
397 proliferation, which was blocked by either DGAT or COX inhibitors (Fig. 8G), demonstrating
398 that DGAT-mediated TAG synthesis and COX-mediated conversion of $cPLA_2\alpha$-released AA
399 into lipid mediators are required for $cPLA_2\alpha$-stimulated A549 lung cancer cell proliferation.
400 Exogenous hGX $sPLA_2$ also stimulated A549 cell proliferation, which was suppressed by
401 inhibition of DGAT and COX (Fig. 8G). Finally, in MDA-MB-231 cells, where DGAT-mediated
402 TAG synthesis was required for $cPLA_2\alpha$-stimulated PGE_2 production (Fig. 5E), $cPLA_2\alpha$
403 overexpression resulted in higher proliferation rates, which were reduced by DGAT inhibition
404 (Fig. 8H). Together, these data demonstrate that LD biogenesis controls both hGX-$sPLA_2$- and
405 $cPLA_2\alpha$-mediated cancer cell proliferation, which is driven by lipid mediators produced by COX
406 and LOX enzymes.
407

408 ## Discussion

409 In this study, we provide evidence that TAG turnover controls the production of a wide range
410 of ω-3 and ω-6 PUFA-derived oxygenated lipid mediators. We show that the esterification of
411 PUFAs into TAGs and their lipolytic release from LDs are necessary for PUFA entry into lipid
412 mediator biosynthetic pathways. We demonstrate that ATGL liberates ω-3 and ω-6 PUFAs
413 from TAGs, alters membrane phospholipid composition and drives lipid mediator production
414 via COX and LOX (Fig. 8I). Our data further suggest that LDs control canonical, PLA_2-induced
415 lipid mediator biosynthesis pathways by sequestering exogenous and membrane-derived
416 PUFAs via DGAT1 and by modulating membrane PUFA content by delivering PUFAs into
417 phospholipids via ATGL. We demonstrate that lipid mediator production induced by hGX
418 $sPLA_2$, which initially releases PUFAs from the plasma membrane and serum lipoproteins,
419 depends on DGAT-driven enrichment of TAGs with PUFAs as well as ATGL-mediated
420 lipolysis. Lipid mediator production induced by $cPLA_2\alpha$, which acts on perinuclear membranes
421 to release AA for eicosanoid production, also depends on intact TAG turnover. These findings
422 change the paradigm of PLA_2-mediated inflammatory and mitogenic signalling by integrating
423 membrane hydrolysis with LD metabolism. Furthermore, inhibition of DGAT-mediated TAG
424 synthesis compromises lipid mediator release from cancer cells, thereby suppressing basal,
425 $sPLA_2$- and $cPLA_2\alpha$-induced cancer cell proliferation and reducing tumour growth in vivo. This
426 study identifies the LD organelle as a central lipid trafficking hub that controls major PUFA
427 supply routes for lipid mediator biosynthesis.
428 One of the most striking findings of the present study is that LD turnover regulates
429 eicosanoid production from both exogenously-added PUFAs and membrane-hydrolysis-

430 derived PUFAs suggesting that the build-up of PUFA-rich TAG stores is a required step in the
431 control of lipid mediator signalling. A similar mechanism has been described in
432 cardiomyocytes, whereby exogenous FAs have to be esterified into TAGs and then released
433 by ATGL to activate peroxisome-proliferator-activated receptor (PPAR) signalling (Haemmerle
434 *et al*, 2011; Zechner *et al*, 2012). Furthermore, as we found DGAT activity to be a prerequisite
435 for both ATGL-induced and $sPLA_2$/$cPLA_2\alpha$-induced eicosanoid production, it can be assumed
436 that LDs control PUFA availability for eicosanoid production through the regulation of both TAG
437 and membrane phospholipid pools.

438 Our previous data showed that breast cancer cells challenged with exogenous PUFAs
439 depend on the balance between DGAT1-mediated sequestration of PUFAs into LDs and their
440 release via ATGL-mediated lipolysis to survive lethal oxidative damage (Jarc *et al*, 2018). In
441 support of this, inhibition of DGAT activity diverts dietary PUFAs towards esterification into
442 membrane phospholipids, thereby increasing their peroxidation and leading to ferroptosis in
443 acidic tumours (Dierge *et al*, 2021). Accordingly, DGAT1 increases the resilience of cancer
444 cells against the stress of increased FA acquisition, which is a hallmark of transformed cells
445 (Wilcock *et al*, 2022). It was recently shown that DGAT1-mediated TAG synthesis is required
446 for prostaglandin formation during macrophage activation (Castoldi *et al*, 2020) and *Drosophila*
447 oogenesis (preprint: Giedt *et al*, 2021). Our results suggest that DGAT activity controls cancer
448 cell growth and proliferation by generating PUFA stores in LDs, which can be used for the
449 production of potent, albeit short-lived, pro-inflammatory and anti-inflammatory lipid signalling
450 molecules. As these signalling molecules are released from cells to act in autocrine and
451 paracrine manners, they can modulate tumour growth by altering the function of cancer cells,
452 immune cells and other cells in the tumour microenvironment (Wang & DuBois, 2010; Greene
453 *et al*, 2011). Thus, in addition to their protective role against nutrient deficiency, lipotoxicity and
454 oxidative stress (Petan, 2020), LDs modulate tumour growth also through the control of lipid
455 mediator-dependent cell-autonomous and non-cell-autonomous mitogenic and inflammatory
456 signalling pathways, and thus emerge as targets for therapeutic intervention. Targeting the
457 DGAT enzymes might improve cancer treatments, particularly under conditions of elevated
458 lipid influx (e.g., abundance of dietary fats, dyslipidemia, oncogene-driven elevated
459 endogenous FA synthesis, high autophagic flux) (Chitraju *et al*, 2017; Nguyen *et al*, 2017;
460 Dierge *et al*, 2021).

461 $sPLA_2$ enzymes display tissue- and cell-specific expression patterns and differ in their
462 membrane binding affinities and hydrolytic activities depending on the phospholipid
463 composition and structural features of their target lipid assemblies (Lambeau & Gelb, 2008;
464 Murakami *et al*, 2020). Their ability to promote lipid mediator production has been attributed
465 either to direct PUFA release from phospholipids (e.g., in the case of hGX $sPLA_2$) or
466 cooperative action with $cPLA_2\alpha$ (e.g., in the case of the group IIA $sPLA_2$) (Hanasaki *et al*, 1999;

467 Bezzine *et al*, 2002; Saiga *et al*, 2005). Regardless of the particular PLA_2(s) involved, the
468 release of PUFAs from phospholipids has been considered the final step in the control of PUFA
469 entry into oxygenation pathways. Here, we show that lipid mediator production by two of the
470 most potent mammalian PLA_2s, hGX $sPLA_2$ and $cPLA_2\alpha$, depends on LD turnover. Notably,
471 hGX-$sPLA_2$-treated MDA-MB-231 breast cancer cells showed an enrichment of both TAGs
472 and phospholipids with PUFAs, but their release from TAGs by ATGL was essential for their
473 conversion into lipid mediators and preceded the action of $cPLA_2\alpha$. Intriguingly, in A549 lung
474 cancer cells, $cPLA_2\alpha$ rather than ATGL was required for hGX-$sPLA_2$-induced PGE_2 production,
475 but intact TAG synthesis was still a prerequisite for both hGX-$sPLA_2$-induced and $cPLA_2\alpha$-
476 induced eicosanoid synthesis and cell proliferation. This suggests that lipid mediator
477 production could be mediated in different cell types by various combinations of PLA_2s and
478 (TAG) lipases, but the LD emerges as a central hub that controls the trafficking and final
479 destination of PUFAs.

480 This study provides a novel view of PLA_2-mediated inflammatory and mitogenic
481 signalling, which integrates membrane hydrolysis with cellular LD metabolism. LDs could be
482 the missing link that will help explain the elusive cross-talk between $sPLA_2$s and $cPLA_2\alpha$ in lipid
483 mediator biosynthesis (Mounier *et al*, 2004; Saiga *et al*, 2005; Lambeau and Gelb, 2008). It
484 will be interesting to investigate in future studies whether LD metabolism governs PLA_2-
485 induced lipid mediator production in various pathophysiological settings. Finally, the hGX
486 $sPLA_2$-induced incorporation of ω-3 and ω-6 PUFAs into TAGs, which is a novel mechanism
487 of enzymatically-induced enrichment of LDs with phospholipid-derived PUFAs, could help
488 clarify the various proposed roles of the group X $sPLA_2$ that extend beyond lipid mediator
489 production (Li *et al*, 2010; Sato *et al*, 2011; Murase *et al*, 2016; Schewe *et al*, 2016; Murakami
490 *et al*, 2020). For example, PUFA-enriched TAGs have been observed in visceral adipose tissue
491 of patients with colorectal cancer, along with elevated expression of hGX $sPLA_2$ and
492 prostaglandin biosynthetic enzymes (Liesenfeld *et al*, 2015).

493 Our results indicate that different cell-type-specific mechanisms might explain the
494 dependence of $cPLA_2\alpha$-induced eicosanoid production on LDs. In the MDA-MB-231 and HeLa
495 cells, $cPLA_2\alpha$ depends on TAG synthesis and ATGL-mediated TAG lipolysis to drive the
496 incorporation of PUFAs into phospholipids, which are then targeted by $cPLA_2\alpha$. In A549 cells,
497 $cPLA_2\alpha$ controls basal and $sPLA_2$-induced PGE_2 production independently of ATGL, although
498 its activity still depends on intact LD biogenesis. In both cases, our data suggest that $cPLA_2\alpha$-
499 mediated AA release for eicosanoid production occurs downstream of, and is controlled by,
500 LD turnover. Interestingly, $cPLA_2\alpha$ has also been shown to drive mitochondrial β-oxidation of
501 both FAs and eicosanoids for energy production (Slatter *et al*, 2016), which is another
502 indication that ATGL and $cPLA_2\alpha$ share common metabolic and signalling pathways.
503 Altogether, our findings suggest that LD turnover regulates the supply of PUFAs for lipid

504 mediator production via at least two pathways: direct delivery of LD-derived PUFAs, which is
505 independent of $cPLA_2\alpha$; and an indirect route, which requires $cPLA_2\alpha$ but depends on LDs for
506 the control of PUFA availability in membrane phospholipids. Notably, our data indicate that
507 other lipases and LD breakdown mechanisms (e.g., lipophagy) besides (or instead of) ATGL
508 might contribute to LD-dependent lipid mediator biosynthesis.

509 One of the intriguing questions that remains to be addressed in future studies is whether
510 PUFA trafficking between the TAG core and the LD phospholipid monolayer is relevant for lipid
511 mediator production. In principle, TAG lipolysis-derived PUFAs can be re-esterified in
512 monolayer phospholipids and targeted by $cPLA_2\alpha$ or other PLA_2s. In agreement with this,
513 $cPLA_2\alpha$, COXs, several prostaglandin synthetases and *de novo* produced eicosanoids have
514 been localised to LDs (Wooten *et al*, 2008; Moreira *et al*, 2009; Bozza *et al*, 2011; Cruz *et al*,
515 2020; Ward *et al*, 2020). In addition, $cPLA_2\alpha$ is involved in remodelling of membrane shape
516 and it might affect LD biogenesis and lipolysis by altering membrane composition and its
517 biophysical properties (Gubern *et al*, 2008; Guijas *et al*, 2014; Antonny *et al*, 2015; Astudillo *et*
518 *al*, 2019; Cao *et al*, 2019; Jarc & Petan, 2020, Zoni *et al*, 2021). In agreement with this, our
519 results indicate that $cPLA_2\alpha$ modulates membrane PUFA-phospholipid content and LD
520 metabolism, including LD abundance and TAG acyl-chain composition. The molecular basis
521 and functional relevance of these findings are currently unclear. We speculate that eicosanoid
522 production does not necessarily occur on LDs as isolated cytosolic platforms, but at specific
523 LD–ER contact sites that enable rapid lipid and protein transfer between the structures
524 involved (i.e., the ER membrane bilayer, the LD phospholipid monolayer and TAG core)
525 (Schuldiner & Bohnert, 2017). Such compartmentalisation would support the interplay among
526 $cPLA_2\alpha$, ATGL and other enzymes in the control of LD turnover, membrane remodelling and
527 the eicosanoid synthesis machinery.

528 In conclusion, our study reveals that LDs are essential for lipid mediator production and
529 cancer cell proliferation. Esterification of PUFAs into TAGs by the DGAT enzymes and PUFA
530 release from LDs (which depends on TAG lipolysis by ATGL, and/or other lipases depending
531 on the cell type) drives lipid mediator production either directly, by feeding PUFAs into the
532 COX/LOX machinery, or by redirecting some of the PUFAs into membrane phospholipids first,
533 whereby they are then targeted by $cPLA_2\alpha$. Notably, both exogenous and $sPLA_2$-membrane-
534 hydrolysis-derived PUFAs have to cycle through LDs to be converted into lipid mediators,
535 which reveals that LDs are optimal storage reservoirs for excess PUFAs that actively control
536 PUFA release. LDs thus have an important regulatory role in lipid mediator production, thereby
537 potentially affecting numerous downstream signalling pathways that are involved in
538 inflammation, immunity and cancer.
539
540

541 # Materials and methods

542 ***Materials***

543 MDA-MB-231 human breast adenocarcinoma cells, A549 human lung carcinoma cells, HeLa
544 human cervical adenocarcinoma cells, C2C12 mouse myoblasts cells, and Caco-2 human
545 colorectal adenocarcinoma cells were obtained from American Type Culture Collection (ATCC,
546 USA). J774A.1 mouse reticulum cell sarcoma macrophages were from the European
547 Collection of Authenticated Cell Cultures (ECACC, UK), and MDA-MB-231 human breast
548 adenocarcinoma cells with stable luciferase 2A and RFP expression (MDA-MB-
549 231/Luciferase-2A-RFP) were from GeneTarget (USA). PC-3 human prostate
550 adenocarcinoma cells were a kind gift from Dr. Mojca Pavlin (University of Ljubljana, Slovenia).
551 OV-90 human ovarian papillary serous adenocarcinoma cells, TOV-112D human ovarian
552 endometrioid carcinoma cells, TOV-21G human ovarian clear cell carcinoma cells and
553 Ishikawa human endometrial adenocarcinoma cells were a kind gift from Dr. Brett McKinnon
554 (Berne University Hospital, Switzerland). SGBS human Simpson-Golabi-Behmel syndrome
555 preadipocytes were a kind gift from Dr. Merce Miranda (Joan XXIII University Hospital
556 Tarragona, Spain), and SH-SY5Y human neuroblastoma cells were a kind gift from Dr. Boris
557 Rogelj (Jožef Stefan Institute, Slovenia). RPMI-1640 culture medium was from ATCC (USA),
558 and Dulbecco's modified Eagle's medium nutrient mixture F-12 (DMEM/F12), DMEM with high
559 glucose and GlutaMAX supplement (DMEM-GlutaMax), foetal bovine serum, Dulbecco's
560 phosphate-buffered saline (DPBS), TrypLE Select and Opti-MEM were from Life Technologies
561 (USA). AA and PGE_2 standards were from Cayman Chemical (USA), and BODIPY 493/503,
562 Lipofectamine RNAiMAX, Lipofectamine 3000, High-capacity cDNA reverse transformation
563 kits were from Thermo Fisher Scientific (USA). Hoechst 33342 nuclear stain was from Enzo
564 Life Sciences (USA). Human ATGL-targeting and $cPLA_2\alpha$-targeting siRNAs and the AllStars
565 Negative Control siRNA were from Qiagen (Germany). T863 (DGAT1 inhibitor), PF-06424439
566 (DGAT2 inhibitor), indomethacin (COX inhibitor), nordihydroguaiaretic acid (LOX inhibitor),
567 essentially fatty acid-free (EFAF) bovine serum albumin (BSA) (cat. no. A7511), FAF-BSA (cat.
568 no. A8806) and Nile red were from Sigma-Aldrich (USA). High Pure RNA isolation kits were
569 from Roche (Germany), horseradish-peroxidase-labelled secondary antibodies were from
570 Jackson ImmunoResearch Laboratories (USA), ATGL antibodies (cat. no. #2138) were from
571 Cell Signaling Technology (USA), $cPLA_2\alpha$ antibodies (cat. no. sc-454) were from Santa Cruz
572 (USA) and β-actin antibodies (cat. no. NB600-532) were from Novus Biologicals (UK).
573 Recombinant wild-type hGX $sPLA_2$ was prepared as described previously (Pucer *et al*, 2013).
574 The full-length cDNAs coding for human $cPLA_2\alpha$ (NCBI RefSeq NM.024420.3) and ATGL
575 (NCBI RefSeq NM.020376.4) were cloned into the pcDNA 4/HisMaxC vector (Thermo Fisher
576 Scientific, USA) using Gibson assembly cloning kits (New England Biolabs, USA), after

577 removal of the N-terminal His-tag region. All of the other chemicals were of at least analytical
578 grade, and were purchased from Sigma-Aldrich (USA) or Serva (Germany).
579
580 ***Cell culture and treatments***
581 MDA-MB-231 cells were cultured in RPMI-1640 medium, A549 cells in DMEM/F12 medium
582 containing 2 mM L-glutamine (Gibco, USA), and HeLa cells in DMEM-Glutamax medium, all
583 supplemented with 10% foetal bovine serum. Adherent cells were detached using TrypLE
584 Select. Unless otherwise indicated, the cells were seeded in 24-well plates at a density of 3
585 $\times 10^4$ (MDA-MB-231), 2.5 $\times 10^4$ (A549) or 1.5 $\times 10^4$ (HeLa) cells/well and grown for 48 h in
586 complete medium, followed by 24 h of serum deprivation in their respective media containing
587 0.02% EFAF-BSA. Aliquots of stock solutions of AA and PGE_2 in absolute ethanol were stored
588 under argon at –80 ºC. Prior to addition to cell cultures, AA was resuspended in the relevant
589 complete medium and incubated for 1 h at room temperature. Unless otherwise indicated,
590 T863 and PF-06424439 were added to cells 2 h before treatments with recombinant hGX
591 $sPLA_2$ (1–10 nM) or AA (10 μM), and were present in the medium for the duration of the
592 treatments. Prior to addition to cell culture, radiolabelled [^{14}C]-OA was saponified by removing
593 ethanol from the stock aliquot of [^{14}C]-OA and resuspending in 50 μL 0.1 mM NaOH. Saponified
594 [^{14}C]-OA was incubated in the relevant complete medium for 30 min at room temperature and
595 stored at –20 ºC.
596
597 ***Silencing of ATGL and $cPLA_2\alpha$ expression using small-interfering RNAs***
598 Reverse transfection was performed in 24-well plates at cell densities of 6 $\times 10^4$ (MDA-MB-
599 231), 5 $\times 10^4$ (A549) or 3 $\times 10^4$ (HeLa) cells/well, or in 6-well plates at 3 $\times 10^5$ (MDA-MB-231),
600 2.5 $\times 10^5$ (A549) or 1.5 $\times 10^5$ (HeLa) cells/well. Gene expression silencing was performed with
601 a 20 nM mixture of two ATGL-specific siRNAs (10 nM each) or a 40 nM mixture of four siRNAs
602 specific for $cPLA_2\alpha$. Non-targeting siRNA controls contained 20 nM (for ATGL) or 40 nM (for
603 $cPLA_2\alpha$) AllStars Negative Control siRNA (Qiagen). Transfection complexes were generated
604 using 1 μL/well Lipofectamine RNAiMAX in 24-well plates, or 7.5 μL/well in 6-well plates, with
605 Opti-MEM medium, according to manufacturer instructions.
606
607 ***Transient overexpression of ATGL and $cPLA_2\alpha$***
608 For transient overexpression experiments, the cells were seeded in complete medium in 24-
609 well plates at a density of 9 $\times 10^4$ (MDA-MB-231), 6 $\times 10^4$ (A549) and 4.5 $\times 10^4$ (HeLa) cells/well,
610 or in 6-well plates at 4.5 $\times 10^5$ (MDA-MB-231), 3 $\times 10^5$ (A549) and 2.5 $\times 10^5$ (HeLa) cells/well.
611 Cells were then incubated for 24 h in complete medium, washed, and transfected with 0.5
612 μg/well plasmid DNA in 24-well plates, or 2.5 μg/well in 6-well plates, using Lipofectamine 3000

613 and Opti-MEM medium, according to manufacturer instructions; they were then left for 6 h in
614 serum-depleted medium containing 0.02% EFAF-BSA (serum starvation). After 6 h, the cells
615 were washed and treated according to the experimental set-up.
616
617 ***Real-time quantitative PCR***
618 Real-time quantitative (q)PCR analysis was performed as described previously (Pucer *et al*,
619 2013; Brglez *et al*, 2014b). Briefly, the cells were seeded in complete medium in 6-well plates
620 at 3 $\times 10^5$ (MDA-MB-231), 2.5 $\times 10^5$ (A549) and 1.5 $\times 10^5$ (HeLa cells) cells/well, grown 48 h in
621 complete medium, followed by 24 h under serum deprivation in medium containing 0.02%
622 EFAF-BSA. Total RNA was isolated from cell lysates and first-strand cDNA was generated
623 using High-Capacity cDNA Reverse Transcription kits (Applied Biosystems, USA), according
624 to the manufacturer instructions. qPCR analysis was performed on a StepOnePlus real-time
625 PCR system (Thermo Scientific, USA) using FastStart Universal SYBR Green Master (Rox;
626 Roche, Switzerland). Calibrator cDNA was transcribed from Quantitative PCR Human
627 Reference Total RNA (Agilent Technologies, USA). Relative gene expression was calculated
628 upon normalisation to two reference genes, considering primer-specific PCR efficiency and
629 error propagation.
630
631 ***Western blotting***
632 The cells were seeded in complete medium in 6-well plates and reverse transfected with
633 siRNAs and/or transiently transfected with pDNA, as described above. Cell lysates were
634 prepared by scrapping adherent cells in Tris-glycine sodium dodecyl sulphate (SDS) sample
635 buffer (2×) (Novex, Life Technologies, USA) that contained 800 mM dithiothreitol (Sigma-
636 Aldrich, USA), with the addition of Halt protease inhibitor cocktail (Thermo Scientific, USA).
637 Lysates were incubated at 95 °C for 10 min and stored on ice. Total protein concentrations
638 were determined using Pierce 660 nm protein assays (Thermo Scientific, USA). Proteins (10–
639 40 μg) were separated on 10% SDS-PAGE gels and then transferred to nitrocellulose
640 membranes (Serva, Germany). The membranes were blocked for 1 h (for ATGL) or 2 h (for
641 $cPLA_2\alpha$) in 5% non-fat dry milk in TBS/0.1% Tween-20 (TBST) or in 1% Western blocking
642 reagent (WBR) (Roche Applied Science, Germany) in TBS (for β-actin), and incubated
643 overnight at 4 °C in the presence of rabbit anti-human primary antibodies for ATGL (1:1000
644 dilution) or mouse anti-human primary antibodies for $cPLA_2\alpha$ (1:250 dilution), both in 5% non-
645 fat dry milk in TBST, or in rabbit anti-human primary antibodies for β-actin (1:5000 dilution) in
646 0.5% WBR in TBS. After washing with TBST, the membranes were incubated for 1 h with
647 horseradish-peroxidase-conjugated secondary antibodies (1:10,000 dilution) in 5% non-fat dry
648 milk in TBST for ATGL, in 0.5% WBR in TBST for $cPLA_2\alpha$, and in 0.5% WBR in TBS for β-

649 actin. The signals were visualised using Lumi-Light Western Blotting Substrate (Roche Applied
650 Science, Germany) on a Gel Doc XR system (Bio-Rad, USA).
651
652 ***Neutral lipid quantification by flow cytometry***
653 Cellular neutral lipid levels were quantified by flow cytometry as described previously (Pucer
654 *et al*, 2013). Floating and adherent cells were harvested and centrifuged at 300× *g* for 10 min,
655 and the pellets were resuspended in 500 µL 1 µg/mL Nile Red solution in DPBS. After a 10-
656 min incubation in the dark, cell analysis was performed by flow cytometry on a FACSCalibur
657 system, equipped with a 488-nm Ar-ion laser, and using the CellQuest software (Becton
658 Dickinson, USA) and an FL-1 (530/30) filter, for at least 2 $\times 10^4$ events per sample.
659
660 ***Triglyceride assays***
661 Cellular TAG contents were determined using TAG assay kits - quantification (Abcam, USA).
662 MDA-MB-231 and HeLa cells were seeded in 6-well plates at 1.5 $\times 10^5$ and 7 $\times 10^4$ cells/well,
663 respectively. After 24 h, MDA-MB-231 cells were treated with 10 nM hGX $sPLA_2$ and HeLa
664 cells with 1 nM hGX $sPLA_2$ in complete medium for 48 h. Cell lysates were prepared and used
665 for TAG quantification according to the manufacturer instructions.
666
667 ***Glycerol release assays***
668 Cellular lipolytic activity was assessed by measuring glycerol release in cell supernatants.
669 Briefly, the cells were reverse transfected and seeded in 48-well plates at a density of 3 $\times 10^4$
670 (MDA-MB-231 cells) or 1.5 $\times 10^4$ cells/well (HeLa cells). For reverse transfection, 0.5 µL
671 Lipofectamine RNAiMAX, 20 nM siRNA and 40 µL OPTI-MEM medium were used per well.
672 After 24 h, the cells were washed, placed in serum-starvation medium containing 0.02% EFAF-
673 BSA, and transfected with 0.250 µg plasmid DNA for protein overexpression using
674 Lipofectamine 3000, according to the manufacturer instructions. After 6 h, the cells were
675 washed and treated with 10 nM hGX $sPLA_2$ for 48 h in complete medium. Cell supernatants
676 were collected in low-binding microcentrifuge tubes and centrifuged for 10 min (4 °C, 16,000×
677 *g*), and the glycerol concentrations were determined using the Glycerol Cell-Based assay kits
678 (Cayman Chemicals, USA), according to the manufacturer instructions.
679
680 ***Untargeted lipidomic analysis of phospholipids and triglycerides***
681 For untargeted lipidomic analysis of hGX $sPLA_2$-induced changes in TAG acyl-chain
682 composition, MDA-MB-231 cells were seeded in complete medium on 10-cm plates at 1 $\times 10^6$
683 cells/plate. After 24 h, the cells were treated with 1 nM hGX $sPLA_2$ in complete medium for 48
684 h. Cell lysates were prepared by washing the cells twice with DPBS and scraping in 1 mL lysis
685 buffer (20 mM Tris-HCl, pH 7.4, 2 mM EDTA, 2 µL Halt protease inhibitor cocktail), followed

686 by centrifugation for 10 min (1000× *g*, 4 °C). Cell pellets were resuspended in 150 µL lysis
687 buffer and sonicated on ice. Total lipids were extracted in chloroform/methanol (2/1, v/v)
688 containing 1% acetic acid, 500 nM butylated hydroxytoluene (BHT) and internal standards (IS;
689 100 pmol 17:0/17:0/17:0 triacylglycerol, Larodan, Solna, Sweden) under constant shaking for
690 1 h (30 rpm/min, 4 °C). After centrifugation at 3300 rpm for 20 min at room temperature, the
691 upper aqueous layer was removed, and the organic solvents were evaporated using a sample
692 concentrator (Techne, UK) equipped with the Dri-Block DB-3 heater (Techne, UK). Lipids were
693 resolved in 200 µL chloroform and stored at –20 ºC. Prior to mass spectrometry, the samples
694 were placed at room temperature and dried and resuspended in 1 mL chloroform/methanol
695 (2/1, v/v). An aliquot of each sample (20 µL) was mixed with 180 µL isopropanol, and 5 µL was
696 used for chromatographic separation on an Acquity-UPLC system (Waters Corporation,
697 Milford, MA, USA), equipped with an ACQUITY BEH C18 column (2.1 × 50 mm, 1.7 µm;
698 Waters Corporation, Milford, MA, USA). A SYNAPT^{TM}G1 qTOF HD mass spectrometer
699 (Waters Corporation, Milford, MA, USA) equipped with an ESI source was used for detection.
700 Data acquisition was carried out using the MassLynx 4.1 software (Waters), and the lipid
701 classes were analysed with the Lipid Data Analyser 1.6.2 software. The data were normalised
702 for recovery, extraction and ionisation efficacy by calculating analyte/internal standard ratios
703 (AU) and expressed as percentage composition.
704 To determine the changes in the phospholipid and TAG profiles in ATGL-depleted and
705 cPLA$_2$α-depleted cells, MDA-MB-231 cells were seeded in complete medium on 6-well plates
706 at 3 ×10^5 cells/well and reverse transfected with ATGL-specific and/or cPLA$_2$α-specific siRNAs,
707 as described above. After 24 h, the cells were washed and grown for 48 h in complete medium
708 in the presence or absence of 10 nM sPLA$_2$. The cells were then washed twice with DPBS and
709 serum starved for the following 24 h in RPMI-1640 medium containing 0.02% EFAF-BSA.
710 Samples were collected (at 0, 3, 24 h of serum starvation) by placing the plates on ice, washing
711 the cells twice with ice-cold DPBS, and scraping the cells in 300 µL lysis buffer, followed by
712 centrifugation for 10 min (1000× *g*, 4 °C). The cell pellets were resuspended in 150 µL lysis
713 buffer and sonicated on ice. Then, 10 µL of each sample was used for protein determination
714 (Pierce 660). Total lipids were extracted by transferring the pellets into 2 ml tubes followed by
715 homogenisation in 700 µL of a 3:1 (v/v) mixture of methyl tert-butyl ether and methanol,
716 containing 1% acetic acid, 500 nM BHT and IS (8 pmol 18:3/18:3/18:3 triacylglycerol, 14:0/14:0
717 phosphatidylcholine, Larodan, Solna, Sweden; 50 pmol 17:0/17:0 phosphatidylethanolamine,
718 12 pmol 17:0/17:0 phosphatidylserine, Avanti Polar Lipids, Alabaster, AL, USA), with two steel
719 beads on a mixer mill (30 Hz, Retsch, Germany) at 4 °C. After homogenisation, the samples
720 were mixed at room temperature under constant shaking for 30 min. Then 140 µL distilled H_2O
721 was added, and the samples were thoroughly mixed and centrifugated (14,000 rpm, 10 min),
722 to establish phase separation. The organic phase (500 µL) was transferred into new tubes and

723 the organic solvent was evaporated off under a stream of nitrogen. The residual protein slurry
724 was dried and used for protein determination after lysis in 400 µL NaOH/SDS (0.3 M/0.1%).
725 Prior to mass spectrometry analysis, the lipids were resolved in 200 µL isopropanol
726 /methanol/H_2O (70/25/10, v/v/v). Chromatographic separation was performed on a 1290
727 Infinity II LC system (Agilent, Santa Clara, CA, USA) equipped with a C18 column (Zorbax
728 RRHD Extend; 2.1 × 50 mm, 1.8 µm; Agilent, Santa Clara, CA, USA), using a 16 min linear
729 gradient from 60% solvent A (H_2O; 10 mM ammonium acetate, 0.1% formic acid, 8 µM
730 phosphoric acid) to 100% solvent B (2-propanol; 10 mM ammonium acetate, 0.1% formic acid,
731 8 µM phosphoric acid). The column compartment was kept at 50 °C. A Q-TOF mass
732 spectrometer (6560 Ion Mobility; Agilent, Santa Clara, CA, USA) equipped with electrospray
733 ionisation source (Dual AJS) was used for detection of the lipids in positive and negative Q-
734 TOF mode. Data acquisition was carried out using the MassHunter Data Acquisition software
735 (B.09; Agilent, Santa Clara, CA, USA). Lipid species were manually identified and lipid data
736 were processed using MassHunter Quantitative Analysis (B.09.00; Agilent, Santa Clara, CA,
737 USA). Data were normalised for recovery, extraction and ionisation efficiency by calculation of
738 the analyte/ internal standard ratios, and are expressed as fmol/µg protein. Lipidomic data
739 were analysed by multiple t-test analysis of log-transformed data to compare two conditions at
740 a time, using GraphPad Prism 9.0.2 (GraphPad Software, USA). Lipid ontology enrichment
741 analysis was performed using the LION/web enrichment and principal component analysis
742 modules (Molenaar *et al*, 2019).
743
744 ***Thin layer chromatography of radiolabelled cellular lipids***
745 MDA-MB-231 cells were seeded in complete medium on T-25 flasks at a density of 5 ×10^5
746 cells/flask. After 24 h, the cells were treated with 1 µCi/sample [^{14}C]-OA for 18 h, washed twice
747 with DPBS, and treated with 10 nM hGX $sPLA_2$ under three different conditions: (a) 24 h in
748 complete medium; (b) 24 h in complete medium followed by 96 h serum deprivation in 0.02%
749 EFAF-BSA in RPMI-1640; and (c) 24 h in 0.02% FAF-BSA in RPMI-1640 followed by 96 h in
750 0.02% EFAF-BSA in RPMI-1640. Lipid extraction was performed with 1 mL hexane/
751 isopropanol (3:2, v/v) under constant shaking for 10 min at room temperature, and repeated
752 twice. The samples were stored in microcentrifuge tubes at –20 ºC. Total proteins were isolated
753 from cell remnants in 2 mL lysis buffer (0.3 M NaOH, 0.1% SDS) under constant shaking for 2
754 h at room temperature. Protein concentrations were determined using BSA standard solutions
755 (Thermo Scientific, USA) and the BCA protein assay reagent (Thermo Scientific, USA).
756 Samples of cellular lipids were dried, resuspended in 20 µL chloroform (repeated three times),
757 and loaded onto the stationary phase of silica TLC plates immobilised on a polymeric binder
758 (Merck, Germany). Dry TLC plates were developed using chloroform/ methanol/ acetone/
759 acetic acid/ H_2O (50/10/20/12/5, v/v/v/v/v) for phospholipid separation, and hexane/ diethyl

760 ether/ acetic acid (70:29:1, v/v/v) for neutral lipid separation. Radiolabelled lipids were detected
761 with autoradiography using an imager (PhosphorImager SI; Amersham Biosciences, UK). To
762 quantify the TAG content, the TLC plates were incubated in an iodine steam, the TAG patches
763 were cut out and placed in vials with scintillation cocktail, and the radioactivity was measured
764 using a liquid scintillation counter (Tri-Carb 1600CA; PerkinElmer, USA).
765
766 ***Lipid mediator analysis using UPLC-MS-MS***
767 MDA-MB-231 cells were seeded in complete medium in 6-well plates at 3×10^5 cells/well. In
768 case of ATGL silencing, cells were reverse transfected with ATGL-specific siRNAs as
769 described above. After 24 h, the cells were treated with 10 nM hGX $sPLA_2$ and/or a mixture of
770 20 μM DGAT1 and 20 μM DGAT2 inhibitors for 48 h, washed with DPBS and left for 24 h in
771 RPMI-1640 medium containing 0.02% EFAF-BSA. Cells with DGAT inhibition were treated
772 with the inhibitors also during the serum starvation phase. The cells were lysed and total
773 protein concentrations were determined as described above. Supernatants were collected in
774 low-binding microcentrifuge tubes, centrifuged at 4 °C (16,000× *g*, 10 min) and stored at –80
775 °C before shipping on dry ice. 1 mL of the supernatants (MDA-MB-231 experiment) were first
776 mixed with 2 mL of ice-cold methanol containing deuterium-labelled internal standards (200
777 nM d8-5S-HETE, d4-LTB_4, d5-LXA_4, d5-RvD2, d4-PGE_2 and 10 μM d8-AA; Cayman
778 Chemical/Biomol GmbH, Hamburg, Germany) to facilitate quantification and sample recovery.
779 Samples were kept at −20 °C for 60 min to allow protein precipitation.
780 Tumour samples for UPLC-MS-MS analysis were collected from mice xenografts. After
781 cancer cell injection and visible tumour growth, mice were subcutaneously treated daily with
782 T863 at a dose of 9.6 mg/kg or corresponding vehicle (0.2% DMSO) for two weeks before
783 being sacrificed and sampled for tumours. Tumour samples (30–50 mg) were weighed and 25
784 μL methanol of each mg tumour was added and then homogenized. After that, samples were
785 centrifuged (16,000× g, 4 °C, 5 min), and 800 μL (corresponding to 32 mg tumour) were filled
786 up to 2 mL methanol and 1 mL PBS was added containing deuterium-labelled internal
787 standards (200 nM d8-5S-HETE, d4-LTB_4, d5-LXA_4, d5-RvD2, d4-PGE_2 and 10 μM d8-AA;
788 Cayman Chemical/Biomol GmbH) to facilitate quantification and sample recovery. Lipid
789 mediator analysis using UPLC-MS-MS was performed as described previously (Werz *et al*,
790 2018) with some minor modifications (Werner *et al*, 2019). Briefly, after centrifugation (1200×
791 *g*, 4 °C, 10 min) 8 mL of acidified H_2O was added (final pH = 3.5) and the samples were
792 subjected to solid phase extraction. The solid phase cartridges (Sep-Pak® Vac 6cc 500 mg/ 6
793 mL C18; Waters, Milford, MA) were equilibrated with 6 mL methanol and then with 2 mL H_2O
794 prior sample loading onto the columns. After washing with 6 mL H_2O and additional 6 mL *n*-
795 hexane, lipid mediators were eluted with 6 mL methyl formate. The eluates were brought to
796 dryness using a TurboVap LV evaporation system (Biotage, Uppsala, Sweden) and

797 resuspended in 200 µL methanol/water (50/50, v/v) for UPLC-MS-MS analysis. Lipid mediator
798 profiling was analyzed with an Acquity™ UPLC system (Waters, Milford, MA, USA) and a
799 QTRAP 5500 Mass Spectrometer (ABSciex, Darmstadt, Germany), equipped with a Turbo V™
800 Source and electrospray ionization. Lipid mediators were separated using an ACQUITY
801 UPLC® BEH C18 column (1.7 µm, 2.1 × 100 mm; Waters, Eschborn, Germany) at 50 °C with
802 a flow rate of 0.3 mL/min and a mobile phase consisting of methanol/water/acetic acid of
803 42/58/0.01 (v/v/v) that was ramped to 86/14/0.01 (v/v/v) over 12.5 min and then to 98/2/0.01
804 (v/v/v) for 3 min (Werner *et al*, 2019). The QTrap 5500 was operated in negative ionization
805 mode using scheduled multiple reaction monitoring (MRM) coupled with information-
806 dependent acquisition. The scheduled MRM window was 60 sec, optimized lipid mediator
807 parameters were adopted (Werner *et al*, 2019), and the curtain gas pressure was set to 35 psi.
808 The retention time and at least six diagnostic ions for each lipid mediator were confirmed by
809 means of external standards (Cayman Chemical/Biomol GmbH). Quantification was achieved
810 by calibration curves for each lipid mediator. Linear calibration curves were obtained for each
811 lipid mediator and gave r^2 values of 0.998 or higher (for fatty acids 0.95 or higher). Additionally,
812 the limit of detection for each targeted lipid mediator was determined (Werner *et al*, 2019).
813

814 ***Quantification of PGE_2 in cell supernatants***

815 The amounts of PGE_2 released into culture medium were routinely determined using a
816 commercial enzyme immunoassay (Prostaglandin E_2 Express ELISA kits; Cayman Chemicals,
817 USA). The cells were seeded in 24-well plates and reverse transfected with siRNAs as
818 described above. After 24 h, the cells were transfected with plasmid DNA as described above
819 and treated with 10 nM hGX $sPLA_2$ and/or 10 µM AA and/or a mixture of 20 µM T863 and 20
820 µM PF-06424439 (DGAT inhibitors) for 48 h in complete medium. The cells were then washed
821 and serum starved for 24 h in the appropriate culture medium containing 0.02% EFAF-BSA.
822 In some experiments, DGAT inhibitors were included in the serum-starvation phase. Cell
823 supernatants were collected in low-binding microcentrifuge tubes, centrifuged at 4 °C (16,000×
824 *g*, 10 min) and immediately used for analysis or stored at –80 °C for up to 7 days. For analysis,
825 50 µL undiluted samples were used, and standard curves prepared by diluting the PGE_2
826 standard in culture medium.
827

828 ***Confocal microscopy***

829 Cytosolic LDs were visualised using BODIPY 493/503 neutral lipid staining. Cells were reverse
830 transfected and seeded on glass-bottomed culture plates at 6 $\times 10^4$ (MDA-MB-231 cells), 3
831 $\times 10^4$ (HeLa cells) and 5 $\times 10^4$ (A549 cells) cells/well. Twenty-four hours later, the media were
832 replaced and the cells were treated with 10 nM hGX $sPLA_2$ and the DGAT inhibitors in complete

833 medium for 48 h, followed by 24-h starvation in serum-free medium containing 0.02% EFAF-
834 BSA. For confocal microscopy, the cells were washed twice with DPBS, stained with 1 μg/mL
835 BODIPY 493/503 and 1 μg/mL Hoechst stain solution in RPMI-1640 medium for 15 min in a
836 CO_2 incubator, washed twice with DPBS, and left in fresh RPMI-1640 medium. Live imaging
837 was carried out at the beginning of and after the 24-h serum starvation using a confocal laser
838 scanning microscope (LSM 710; Carl Zeiss, Germany) and a stage-top microscope CO_2
839 incubation system (Tokai Hit, Japan). Images were processed using the Zen software (Carl
840 Zeiss, Germany).
841
842 ***LD counting and diameter analysis***
843 Confocal microscopy images of BODIPY 493/503 stained LDs were used for computer image
844 analysis with the ImageJ software (National Institutes of Health, USA) and the LD Counter
845 Plugin (https://doi.org/10.5281/zenodo.2581434). Analysis was performed on 32-bit two-
846 dimensional images, whereby the numbers and sizes of the LDs were determined according
847 to the plugin instructions. LD diameters were calculated from the LD surface areas. Analyses
848 were performed on at least 40 cells/sample. Data were loaded into the Prism 9.0.2 software
849 (GraphPad Software, USA), with the geometric means of the LD diameters and numbers
850 calculated per individual cell in the samples, followed by the statistical analysis.
851
852 ***Cell proliferation***
853 MDA-MB-231/Luciferase-2A-RFP cells were seeded in complete medium in 96-well plates at
854 5×10^3 cells/well in at least triplicates. After 24 h, the cells were treated with 20 μM DGAT1 and
855 20 μM DGAT2 inhibitors and/or 1 μM PGE_2 and/or 10 nM hGX $sPLA_2$ as described above, and
856 left in complete medium for 72 h. PGE_2 was replenished every 24 h by direct addition to the
857 culture medium. In transient transfection experiments, the cells were seeded in complete
858 medium on 48-well plates at 3×10^4 (MDA-MB-231/Luciferase-2A-RFP cells) or 1.5×10^4 (A549
859 cells) cells/well. After 24 h, the cells were washed and transfected with 0.250 μg plasmid
860 DNA/well using 0.5 μL P3000 reagent and 1 μL Lipofectamine 3000 in OptiMEM medium, and
861 incubated in RPMI-1640 (MDA-MB-231) or DMEM/F12 with 2 mM L-glutamine (A549)
862 containing 0.02% EFAF-BSA. After 6 h, the cells were treated with 10 nM recombinant hGX
863 $sPLA_2$ in complete medium, with 25 μM (A549) or 50 μM (MDA-MB-231) indomethacin, 25 μM
864 nordihydroguaiaretic acid, and/or 20 μM each of the T863 and PF-06424439 DGAT1 and
865 DGAT2 inhibitors, respectively. A549 cell proliferation was determined after 48 h using the
866 direct cell proliferation assay kits (CyQUANT; Invitrogen, USA). MDA-MB-231/Luciferase-2A-
867 RFP cell proliferation was determined by measuring RFP fluorescence emission (excitation,
868 558 nm; emission, 583 nm) on a microplate reader (Infinite M1000; Tecan, Austria). The final

869 data were obtained after subtracting the background signal of the blank samples that contained
870 culture medium without cells.
871
872 ***Clonogenic assay***
873 MDA-MB-231 cells were seeded in 24-well plates in complete medium as described above.
874 After 24 h, the cells were treated with 20 μM T863 and/or 20 μM PF-06424439 and left for 24
875 h. Cells were then washed and harvested for cell counting. 500 cells/well were seeded in 6-
876 well plates and colony formation followed for nine days in complete medium containing 20 μM
877 T863 and/or 20 μM PF-06424439. Medium was replaced every 48–72 h. For analysis, colonies
878 were washed with DPBS, fixed in 100% cold methanol at 4 °C for 15 min and stained with
879 0.5% crystal violet in DBPS. Images were taken for colony counting with ImageJ software
880 (National Institutes of Health, USA).
881
882 ***Mouse studies***
883 All animal experiments were performed according to the directives of the EU 2010/63 and were
884 approved by the Administration of the Republic of Slovenia for Food Safety, Veterinary and
885 Plant Protection of the Ministry of Agriculture, Forestry and Foods, Republic of Slovenia (Permit
886 Number U34401-9/2020/9). Laboratory animals were housed in IVC cages (Techniplast), fed
887 standard chow (Mucedola) and tap water was provided ab libitum. Mice were maintained in
888 12-12 h dark-light cycle at approximately 40–60% relative humidity and an ambient
889 temperature of 22 °C. All animals used in the study were healthy and accompanied with health
890 certificate from the animal vendor. Health status was confirmed by FELASA recommended
891 Mouse Vivum immunocompetent panel (QM Diagnostics). To test the anti-tumour effect of
892 DGAT1 inhibition, female 8–10 weeks old SCID C.B-17/IcrHsd-*Prkdc*^{scid} mice (Envigo, Italy)
893 were used for xenograft cancer studies. 3×10^{6} MDA-MB-231/Luciferase-2A-RFP cells were
894 implanted into the right flank of the mouse. When a certain tumour dimension reached 5 mm,
895 subcutaneous daily treatments were started with T863 at a dose of 9.6 mg/kg or with
896 corresponding 0.2% DMSO vehicle. Body weight and tumour size via calliper measurements
897 were performed every couple of days. Tumour burden was calculated using the formula
898 $V=(a*b*c*\Pi)/6$. Animals were humanely euthanized either when the observed tumour
899 dimension reached 12 mm, the tumour ulcerated or when animals lost over 20% of their own
900 body mass. Tumour samples at the end of the experiment were collected and snap frozen in
901 liquid nitrogen for further UPLC-MS-MS analysis.
902
903 ***Statistical analysis***
904 Statistical analyses were performed using Prism 9.0.2 (GraphPad Software, USA). Unless
905 otherwise indicated, the data are presented as means ±SEM of at least three independent

experiments. Statistical significance was determined using t-tests, one-way or two-way ANOVA, followed by Bonferroni, Sidak or Tukey's multiple comparison tests. P values <0.05 were considered as statistically significant.

Acknowledgements

We are grateful to Ana Temprano Lopez, Petra Hruševar, Ana Kump, Ema Guštin and Belen Vilanova Baeza for their technical help, Dr. Mojca Pavlin (University of Ljubljana, Slovenia), Dr. Brett McKinnon (Berne University Hospital, Switzerland), Dr. Merce Miranda (Joan XXIII University Hospital Tarragona, Spain) and Dr. Boris Rogelj (Jožef Stefan Institute, Slovenia) for kindly providing cell lines. We thank Dr. Chris Berrie for critical reading of the manuscript. This work was supported by the Slovenian Research Agency young researcher (1000-15-106) and postdoctoral grants (Z3-2650) to E.J.J., the P1-0207 Programme grant, and J7-1818 Project grant to T.P., P4-0176 Programme grant to R.J. and J4-4563 Project grant to D.L.; by the Deutsche Forschungsgemeinschaft (DFG, German Research Foundation), Project-ID 239748522 - SFB 1127 ChemBioSys, and the EU COST Action CA19105 EpiLipidNet.

Author contributions

E.J.J. performed most of the experiments, analysed the data, and prepared manuscript draft; A.P.J. and V.B. performed initial lipidomic experiments; Š.K. prepared samples for lipid mediator mass spectrometry analysis and performed LD diameter analysis; T.O.E. performed mass spectrometry analyses, designed experiments, contributed ideas and revised the paper; R.Z. provided materials, designed experiments, contributed ideas and revised the paper; G.L. contributed materials, ideas and revised the paper; P.M.J., J.G. and O.W. performed lipid mediator mass spectrometry analyses and revised the paper; D.L. and A.G.U. performed in vivo studies, and R.J. revised the paper; T.P. conceptualised the study, analysed the data, prepared the figures and illustrations, and wrote the manuscript.

Conflicts of interest

The authors declare that they have no conflicts of interest.

References

Accioly MT, Pacheco P, Maya-Monteiro CM, Carrossini N, Robbs BK, Oliveira SS, Kaufmann C, Morgado-Diaz JA, Bozza PT & Viola JPB (2008) Lipid bodies are reservoirs of

941 cyclooxygenase-2 and sites of prostaglandin E_2 synthesis in colon cancer cells. *Cancer*
942 *Res* 68: 1732–1740
943 Ackerman D, Tumanov S, Qiu B, Michalopoulou E, Spata M, Azzam A, Xie H, Simon MC &
944 Kamphorst JJ (2018) Triglycerides promote lipid homeostasis during hypoxic stress by
945 balancing fatty acid saturation. *Cell Reports* 24: 2596–2605.e5
946 Al-Zoughbi W, Pichler M, Gorkiewicz G, Guertl-Lackner B, Haybaeck J, Jahn SW, Lackner C,
947 Liegl-Atzwanger B, Popper H, Schauer S, *et al* (2016) Loss of adipose triglyceride lipase
948 is associated with human cancer and induces mouse pulmonary neoplasia. *Oncotarget* 7:
949 33832–33840.
950 Antonny B, Vanni S, Shindou H & Ferreira T (2015) From zero to six double bonds:
951 phospholipid unsaturation and organelle function. *Trends Cell Biol* 25: 427–436
952 Astudillo AM, Balboa MA & Balsinde J (2019) Selectivity of phospholipid hydrolysis by
953 phospholipase A_2 enzymes in activated cells leading to polyunsaturated fatty acid
954 mobilization. *Biochim Biophys Acta - Mol Cell Biol Lipids* 1864: 772–783.
955 Bailey AP, Koster G, Guillermier C, Hirst EMA, MacRae JI, Lechene CP, Postle AD & Gould
956 AP (2015) Antioxidant role for lipid droplets in a stem cell niche of *Drosophila*. *Cell* 163:
957 340–353
958 Bezzine S, Bollinger JG, Singer AG, Veatch SL, Keller SL & Gelb MH (2002) On the binding
959 preference of human groups IIA and X phospholipases A_2 for membranes with anionic
960 phospholipids. *J Biol Chem* 277: 48523–48534
961 Bonventre J (2004) Cytosolic phospholipase A_2alpha reigns supreme in arthritis and bone
962 resorption. *Trends Immunol* 25, 116–119
963 Bosch M, Parton RG & Pol A (2020) Lipid droplets, bioenergetic fluxes, and metabolic flexibility.
964 *Semin Cell Dev Biol* 108: 33–46
965 Bosch M, Sweet MJ, Parton RG & Pol A (2021) Lipid droplets and the host–pathogen dynamic:
966 FATal attraction? *J Cell Biol* 220: e202104005
967 Bozza PT, Bakker-Abreu I, Navarro-Xavier RA & Bandeira-Melo C (2011) Lipid body function
968 in eicosanoid synthesis: an update. *Prostaglandins Leukot Essent Fatty Acids* 85: 205–
969 213
970 Brglez V, Lambeau G & Petan T (2014a) Secreted phospholipases A_2 in cancer: diverse
971 mechanisms of action. *Biochimie* 107 Pt A: 114–23
972 Brglez V, Pucer A, Pungerčar J, Lambeau G & Petan T (2014b) Secreted phospholipases A_2
973 are differentially expressed and epigenetically silenced in human breast cancer cells.
974 *Biochem Biophys Res Commun* 445: 230–235
975 Brok MH den, Raaijmakers TK, Collado-Camps E & Adema GJ (2018) Lipid droplets as
976 immune modulators in myeloid cells. *Trends Immunol* 39: 380–392

977 Cao J, Zhou Y, Peng H, Huang X, Stahler S, Suri V, Qadri A, Gareski T, Jones J, Hahm S, *et*
978 *al* (2011) Targeting acyl-CoA:diacylglycerol acyltransferase 1 (DGAT1) with small
979 molecule inhibitors for the treatment of metabolic diseases. *J Biol Chem* 286: 41838–
980 41851
981 Cao Z, Hao Y, Fung CW, Lee YY, Wang P, Li X, Xie K, Lam WJ, Qiu Y, Tang BZ, *et al* (2019)
982 Dietary fatty acids promote lipid droplet diversity through seipin enrichment in an ER
983 subdomain. *Nat Commun* 10: 2902
984 Castoldi A, Monteiro LB, Bakker N van T, Sanin DE, Rana N, Corrado M, Cameron AM,
985 Hässler F, Matsushita M, Caputa G, *et al* (2020) Triacylglycerol synthesis enhances
986 macrophage inflammatory function. *Nat Commun* 11: 4107
987 Cheng X, Geng F, Pan M, Wu X, Zhong Y, Wang C, Tian Z, Cheng C, Zhang R, Puduvalli V,
988 *et al* (2020) Targeting DGAT1 ameliorates glioblastoma by increasing fat catabolism and
989 oxidative stress. *Cell Metab* 32: 229–242.e8
990 Chitraju C, Mejhert N, Haas JT, Diaz-Ramirez LG, Grueter CA, Imbriglio JE, Pinto S, Koliwad
991 SK, Walther TC & Farese RV (2017) Triglyceride synthesis by DGAT1 protects adipocytes
992 from lipid-induced ER stress during lipolysis. *Cell Metab* 26: 407–418.e3
993 Coleman RA & Mashek DG (2011) Mammalian triacylglycerol metabolism: synthesis, lipolysis,
994 and signaling. *Chem Rev* 111: 6359–6386
995 Cruz ALS, Barreto E de A, Fazolini NPB, Viola JPB & Bozza PT (2020) Lipid droplets: platforms
996 with multiple functions in cancer hallmarks. *Cell Death Dis* 11: 105
997 Dennis EA & Norris PC (2015) Eicosanoid storm in infection and inflammation. *Nat Rev*
998 *Immunol* 15: 511–523
999 Dichlberger A, Schlager S, Maaninka K, Schneider WJ & Kovanen PT (2014) Adipose
1000 triglyceride lipase regulates eicosanoid production in activated human mast cells. *J Lipid*
1001 *Res* 55: 2471–2478
1002 Dierge E, Debock E, Guilbaud C, Corbet C, Mignolet E, Mignard L, Bastien E, Dessy C,
1003 Larondelle Y & Feron O (2021) Peroxidation of n-3 and n-6 polyunsaturated fatty acids in
1004 the acidic tumor environment leads to ferroptosis-mediated anticancer effects. *Cell Metab*
1005 33: 1701–1715.e5
1006 Dvorak AM, Dvorak HF, Peters SP, Shulman ES, MacGlashan DW, Pyne K, Harvey VS, Galli
1007 SJ & Lichtenstein LM (1983) Lipid bodies: cytoplasmic organelles important to
1008 arachidonate metabolism in macrophages and mast cells. *J Immunol* 131: 2965–2976
1009 Duchez A-C, Boudreau LH, Naika GS, Rousseau M, Cloutier N, Levesque T, Gelb MH &
1010 Boilard E (2019) Respective contribution of cytosolic phospholipase A2α and secreted
1011 phospholipase A_2 IIA to inflammation and eicosanoid production in arthritis. *Prostaglandins*
1012 *Other Lipid Mediat* 143: 106340

1013 Eichmann TO, Kumari M, Haas JT, Farese RV, Zimmermann R, Lass A & Zechner R (2012)
1014 Studies on the substrate and stereo/ regioselectivity of adipose triglyceride lipase,
1015 hormone-sensitive lipase, and diacylglycerol-O-acyltransferases. *J Biol Chem* 287:
1016 41446–41457
1017 Futatsugi K, Kung DW, Orr STM, Cabral S, Hepworth D, Aspnes G, Bader S, Bian J, Boehm
1018 M, Carpino PA, *et al* (2015) Discovery and optimization of imidazopyridine-based inhibitors
1019 of diacylglycerol acyltransferase 2 (DGAT2). *J Med Chem* 58: 7173–7185
1020 Gartung A, Zhao J, Chen S, Mottillo E, VanHecke GC, Ahn Y-H, Maddipati KR, Sorokin A,
1021 Granneman J & Lee M-J (2016) Characterization of eicosanoids produced by adipocyte
1022 lipolysis: implication of cyclooxygenase-2 in adipose inflammation. *J Biol Chem* 291:
1023 16001–16010
1024 Giedt MS, Thomalla JM, Johnson MR, Lai ZW, Tootle TL & Welte MA (2021) Adipose
1025 triglyceride lipase promotes prostaglandin-dependent actin remodeling by regulating
1026 substrate release from lipid droplets. Preprint at *bioRxiv* 2021.08.02.454724
1027 doi: https://doi.org/10.1101/2021.08.02.454724.
1028 Greenberg AS, Coleman RA, Kraemer FB, McManaman JL, Obin MS, Puri V, Yan Q-W,
1029 Miyoshi H & Mashek DG (2011) The role of lipid droplets in metabolic disease in rodents
1030 and humans. *J Clin Invest* 121: 2102–2110
1031 Greene ER, Huang S, Serhan CN & Panigrahy D (2011) Regulation of inflammation in cancer
1032 by eicosanoids. *Prostag Other Lipid Mediat* 96: 27–36
1033 Gubern A, Casas J, Barceló-Torns M, Barneda D, Rosa X de la, Masgrau R, Picatoste F,
1034 Balsinde J, Balboa MA & Claro E (2008) Group IVA phospholipase A_2 is necessary for the
1035 biogenesis of lipid droplets. *J Biol Chem* 283: 27369–27382
1036 Guillaume C, Payré C, Jemel I, Jeammet L, Bezzine S, Naika GS, Bollinger J, Grellier P, Gelb
1037 MH, Schrével J, *et al* (2015) In vitro anti-*Plasmodium falciparum* properties of the full set
1038 of human secreted phospholipases A_2. *Infect Immun* 83: 2453–2465
1039 Guijas C, Rodríguez JP, Rubio JM, Balboa MA & Balsinde J (2014) Phospholipase A_2
1040 regulation of lipid droplet formation. *Biochim Biophys Acta* 1841: 1661–1671
1041 Haemmerle G, Moustafa T, Woelkart G, Büttner S, Schmidt A, Weijer T van de, Hesselink M,
1042 Jaeger D, Kienesberger PC, Zierler K, *et al* (2011) ATGL-mediated fat catabolism
1043 regulates cardiac mitochondrial function via PPAR-α and PGC-1. *Nat Med* 17: 1076–1085
1044 Hanasaki K, Ono T, Saiga A, Morioka Y, Ikeda M, Kawamoto K, Higashino K, Nakano K,
1045 Yamada K, Ishizaki J & Arita H (1999) Purified group X secretory phospholipase A_2 induced
1046 prominent release of arachidonic acid from human myeloid leukemia cells. *J Biol Chem*
1047 274: 34203–34211

1048 Hayashi D, Mouchlis VD & Dennis EA (2021) Omega-3 *versus* omega-6 fatty acid availability
1049 is controlled by hydrophobic site geometries of phospholipase A_2s. *J Lipid Res* 62: 100113
1050 doi: 10.1016/j.jlr.2021.100113 [paper in press]
1051 Henne WM, Reese ML & Goodman JM (2018) The assembly of lipid droplets and their roles
1052 in challenged cells. *EMBO J* 37: e98947
1053 Jarc E, Kump A, Malavašič P, Eichmann TO, Zimmermann R & Petan T (2018) Lipid droplets
1054 induced by secreted phospholipase A_2 and unsaturated fatty acids protect breast cancer
1055 cells from nutrient and lipotoxic stress. *Biochim Biophys Acta - Mol Cell Biol Lipids* 1863:
1056 247–265
1057 Jarc E & Petan T (2020) A twist of FATe: lipid droplets and inflammatory lipid mediators.
1058 *Biochimie* 169: 69–87
1059 Koliwad SK, Streeper RS, Monetti M, Cornelissen I, Chan L, Terayama K, Naylor S, Rao M,
1060 Hubbard B & Farese RV (2010) DGAT1-dependent triacylglycerol storage by
1061 macrophages protects mice from diet-induced insulin resistance and inflammation. *J Clin*
1062 *Invest* 120: 756–767
1063 Koundouros N, Karali E, Tripp A, Valle A, Inglese P, Perry NJS, Magee DJ, Virmouni SA, Elder
1064 GA, Tyson AL, *et al* (2020) Metabolic fingerprinting links oncogenic PIK3CA with enhanced
1065 arachidonic-acid-derived eicosanoids. *Cell* 181: 1596–1611.e27
1066 Kudo K, Miki Y, Carreras J, Nakayama S, Nakamoto Y, Ito M, Nagashima E, Yamamoto K,
1067 Higuchi H, Morita S, *et al* (2022) Secreted phospholipase A2 modifies extracellular
1068 vesicles and accelerates B cell lymphoma. *Cell Metab* 34: 615-633.e8
1069 Lambeau G & Gelb MH (2008) Biochemistry and physiology of mammalian secreted
1070 phospholipases A_2. *Annu Rev Biochem* 77: 495–520
1071 Leslie CC (2015) Cytosolic phospholipase A_2: physiological function and role in disease. *J Lipid*
1072 *Res* 56: 1386–1402
1073 Li X, Shridas P, Forrest K, Bailey W & Webb NR (2010) Group X secretory phospholipase A_2
1074 negatively regulates adipogenesis in murine models. *FASEB J* 24: 4313–4324
1075 Liesenfeld DB, Grapov D, Fahrmann JF, Salou M, Scherer D, Toth R, Habermann N, Bohm J,
1076 Schrotz-King P, Gigic B, *et al* (2015) Metabolomics and transcriptomics identify pathway
1077 differences between visceral and subcutaneous adipose tissue in colorectal cancer
1078 patients: the ColoCare study. *Am J Clin Nutrition* 102: 433–443
1079 Listenberger LL, Han X, Lewis SE, Cases S, Farese RV, Ory DS & Schaffer JE (2003)
1080 Triglyceride accumulation protects against fatty acid-induced lipotoxicity. *Proc Natl Acad*
1081 *Sci U S A* 100: 3077–3082
1082 Molenaar MR, Jeucken A, Wassenaar TA, van de Lest CHA, Brouwers JF & Helms JB (2019)
1083 LION/web: a web-based ontology enrichment tool for lipidomic data analysis. *Gigascience*
1084 8: giz061

1085 Moreira LS, Piva B, Gentile LB, Mesquita-Santos FP, D'Avila H, Maya-Monteiro CM, Bozza
1086 PT, Bandeira-Melo C & Diaz BL (2009) Cytosolic phospholipase A_2-driven PGE2 synthesis
1087 within unsaturated fatty acids-induced lipid bodies of epithelial cells. *Biochim Biophys Acta*
1088 *- Mol Cell Biology Lipids* 1791: 156–165
1089 Mounier CM, Ghomashchi F, Lindsay MR, James S, Singer AG, Parton RG & Gelb MH (2004)
1090 Arachidonic acid release from mammalian cells transfected with human groups IIA and X
1091 secreted phospholipase A_2 occurs predominantly during the secretory process and with
1092 the involvement of cytosolic phospholipase A_2-α. *J Biol Chem* 279: 25024–25038
1093 Murakami M, Sato H & Taketomi Y (2020) Updating phospholipase A_2 biology. *Biomolecules*
1094 10: 1457
1095 Murakami M, Taketomi Y, Miki Y, Sato H, Hirabayashi T & Yamamoto K (2011) Recent
1096 progress in phospholipase A_2 research: from cells to animals to humans. *Prog Lipid Res*
1097 50: 152–192
1098 Murase R, Sato H, Yamamoto K, Ushida A, Nishito Y, Ikeda K, Kobayashi T, Yamamoto T,
1099 Taketomi Y & Murakami M (2016) Group X secreted phospholipase A_2 releases ω3
1100 polyunsaturated fatty acids, suppresses colitis, and promotes sperm fertility. *J Biol Chem*
1101 291: 6895–6911
1102 Nguyen TB, Louie SM, Daniele JR, Tran Q, Dillin A, Zoncu R, Nomura DK & Olzmann JA
1103 (2017) DGAT1-dependent lipid droplet biogenesis protects mitochondrial function during
1104 starvation-induced autophagy. *Dev Cell* 42: 9–21.e5
1105 Nieman KM, Kenny HA, Penicka CV, Ladanyi A, Buell-Gutbrod R, Zillhardt MR, Romero IL,
1106 Carey MS, Mills GB, Hotamisligil GS, *et al* (2010) Adipocytes promote ovarian cancer
1107 metastasis and provide energy for rapid tumor growth. *Nat Med* 17: 1498–1503
1108 Nomura DK, Lombardi DP, Chang JW, Niessen S, Ward AM, Long JZ, Hoover HH & Cravatt
1109 BF (2011) Monoacylglycerol lipase exerts dual control over endocannabinoid and fatty acid
1110 pathways to support prostate cancer. *Chem Biol* 18: 846–856
1111 Nomura DK, Long JZ, Niessen S, Hoover HS, Ng S-W & Cravatt BF (2010) Monoacylglycerol
1112 lipase regulates a fatty-acid network that promotes cancer pathogenesis. *Cell* 140: 49–61
1113 Ogden HL, Lai Y, Nolin JD, An D, Frevert CW, Gelb MH, Altemeier WA & Hallstrand TS (2020)
1114 Secreted phospholipase A_2 group X acts as an adjuvant for type 2 inflammation, leading
1115 to an allergen-specific immune response in the lung. *J Immunol* 204: 3097–3107
1116 Olzmann JA & Carvalho P (2019) Dynamics and functions of lipid droplets. *Nat Rev Mol Cell*
1117 *Biology* 20: 137–155
1118 Pereira-Dutra FS, Teixeira L, Costa MFS & Bozza PT (2019) Fat, fight, and beyond: the
1119 multiple roles of lipid droplets in infections and inflammation. *J Leukocyte Biol* 106: 563–
1120 580

1121 Pérez-Chacón G, Astudillo AM, Balgoma D, Balboa MA & Balsinde J (2009) Control of free
1122 arachidonic acid levels by phospholipases A_2 and lysophospholipid acyltransferases.
1123 *Biochim Biophys Acta - Mol Cell Biology Lipids* 1791: 1103–1113
1124 Petan T (2020) Lipid droplets in cancer. *Rev Physiol Biochem Pharmacol.* Springer, Berlin,
1125 Heidelberg. https://doi.org/10.1007/112_2020_51 [paper in press]
1126 Pucer A, Brglez V, Payré C, Pungerčar J, Lambeau G & Petan T (2013) Group X secreted
1127 phospholipase A_2 induces lipid droplet formation and prolongs breast cancer cell survival.
1128 *Mol Cancer* 12: 111
1129 Rambold AS, Cohen S & Lippincott-Schwartz J (2015) Fatty-acid trafficking in starved cells:
1130 regulation by lipid droplet lipolysis, autophagy, and mitochondrial fusion dynamics. *Dev*
1131 *Cell* 32: 678–692
1132 Riederer M, Lechleitner M, Köfeler H & Frank S (2017) Reduced expression of adipose
1133 triglyceride lipase decreases arachidonic acid release and prostacyclin secretion in human
1134 aortic endothelial cells. *Arch Physiol Biochem* 123: 249–253
1135 Röhrig F & Schulze A (2016) The multifaceted roles of fatty acid synthesis in cancer. *Nat Rev*
1136 *Cancer* 16: 732–749
1137 Saiga A, Uozumi N, Ono T, Seno K, Ishimoto Y, Arita H, Shimizu T & Hanasaki K (2005) Group
1138 X secretory phospholipase A2 can induce arachidonic acid release and eicosanoid
1139 production without activation of cytosolic phospholipase A2 alpha. *Prostaglandins Other*
1140 *Lipid Mediat* 75: 79–89
1141 Sato H, Isogai Y, Masuda S, Taketomi Y, Miki Y, Kamei D, Hara S, Kobayashi T, Ishikawa Y,
1142 Ishii T, *et al* (2011) Physiological roles of group X-secreted phospholipase A_2 in
1143 reproduction, gastrointestinal phospholipid digestion, and neuronal function. *J Biol Chem*
1144 286: 11632–11648
1145 Sato H, Taketomi Y, Miki Y, Murase R, Yamamoto K & Murakami M (2020) Secreted
1146 phospholipase PLA2G2D contributes to metabolic health by mobilizing ω3
1147 polyunsaturated fatty acids in WAT. *Cell Reports* 31: 107579
1148 Schewe M, Franken PF, Sacchetti A, Schmitt M, Joosten R, Böttcher R, Royen ME van,
1149 Jeammet L, Payré C, Scott PM, *et al* (2016) Secreted phospholipases A_2 are intestinal
1150 stem cell niche factors with distinct roles in homeostasis, inflammation, and cancer. *Cell*
1151 *Stem Cell* 19: 38–51
1152 Schlager S, Goeritzer M, Jandl K, Frei R, Vujic N, Kolb D, Strohmaier H, Dorow J, Eichmann
1153 TO, Rosenberger A, *et al* (2015) Adipose triglyceride lipase acts on neutrophil lipid droplets
1154 to regulate substrate availability for lipid mediator synthesis. *J Leukocyte Biol* 98: 837–850
1155 Schlager S, Vujic N, Korbelius M, Duta-Mare M, Dorow J, Leopold C, Rainer S, Wegscheider
1156 M, Reicher H, Ceglarek U, *et al* (2017) Lysosomal lipid hydrolysis provides substrates for
1157 lipid mediator synthesis in murine macrophages. *Oncotarget* 8: 40037–40051

1158 Schuldiner M & Bohnert M (2017) A different kind of love - lipid droplet contact sites. *Biochim*
1159 *Biophys Acta* 1862: 1188–1196
1160 Schweiger M, Romauch M, Schreiber R, Grabner GF, Hütter S, Kotzbeck P, Benedikt P,
1161 Eichmann TO, Yamada S, Knittelfelder O, *et al* (2017) Pharmacological inhibition of
1162 adipose triglyceride lipase corrects high-fat diet-induced insulin resistance and
1163 hepatosteatosis in mice. *Nat Commun* 8: 14859
1164 Shimizu T (2009) Lipid mediators in health and disease: enzymes and receptors as therapeutic
1165 targets for the regulation of immunity and inflammation. *Annu Rev Pharmacol* 49: 123–150
1166 Shridas P, Bailey WM, Boyanovsky BB, Oslund RC, Gelb MH & Webb NR (2010) Group X
1167 secretory phospholipase A_2 regulates the expression of steroidogenic acute regulatory
1168 protein (StAR) in mouse adrenal glands. *J Biol Chem* 285: 20031–20039
1169 Slatter DA, Aldrovandi M, O'Connor A, Allen SM, Brasher CJ, Murphy RC, Mecklemann S,
1170 Ravi S, Darley-Usmar V & O'Donnell VB (2016) Mapping the human platelet lipidome
1171 reveals cytosolic phospholipase A_2 as a regulator of mitochondrial bioenergetics during
1172 activation. *Cell Metab* 23: 930–944
1173 Smirnova E, Goldberg EB, Makarova KS, Lin L, Brown WJ & Jackson CL (2005) ATGL has a
1174 key role in lipid droplet/adiposome degradation in mammalian cells. *EMBO Rep* 7: 106–
1175 113
1176 Sohn JH, Lee YK, Han JS, Jeon YG, Kim JI, Choe SS, Kim SJ, Yoo HJ & Kim JB (2018)
1177 Perilipin 1 (Plin1) deficiency promotes inflammatory responses in lean adipose tissue
1178 through lipid dysregulation. *J Biol Chem* 293: 13974–13988
1179 Surrel F, Jemel I, Boilard E, Bollinger JG, Payré C, Mounier CM, Talvinen KA, Laine VJO,
1180 Nevalainen TJ, Gelb MH, *et al* (2009) Group X phospholipase A_2 stimulates the
1181 proliferation of colon cancer cells by producing various lipid mediators. *Mol Pharmacol* 76:
1182 778–790
1183 Thiam AR & Ikonen E (2020) Lipid droplet nucleation. *Trends Cell Biol* 31: 108–118
1184 Triggiani M, Oriente A & Marone G (1994) Differential roles for triglyceride and phospholipid
1185 pools of arachidonic acid in human lung macrophages. *J Immunol* 152: 1394–1403
1186 Walther TC, Chung J & Farese RV (2017) Lipid droplet biogenesis. *Annu Rev Cell Dev Biol*
1187 33: 491–510
1188 Wang D & DuBois RN (2010) Eicosanoids and cancer. *Nat Rev Cancer* 10: 181–193
1189 Wang YY, Attané C, Milhas D, Dirat B, Dauvillier S, Guerard A, Gilhodes J, Lazar I, Alet N,
1190 Laurent V, *et al* (2017) Mammary adipocytes stimulate breast cancer invasion through
1191 metabolic remodeling of tumor cells. *JCI Insight* 2: e87489
1192 Ward KE, Ropa JP, Adu-Gyamfi E & Stahelin RV (2012) C2 domain membrane penetration by
1193 group IVA cytosolic phospholipase A_2 induces membrane curvature changes. *J Lipid Res*
1194 53: 2656–2666

1195 Ward KE, Sengupta R, Ropa JP, Amiar S & Stahelin ARV (2020) The cytosolic phospholipase
1196 $A_2\alpha$ N-terminal C2 domain binds and oligomerizes on membranes with positive curvature.
1197 *Biomolecules* 10: 647
1198 Welte MA & Gould AP (2017) Lipid droplet functions beyond energy storage. *Biochim Biophys*
1199 *Acta* 1862: 1260–1272
1200 Werner M, Jordan PM, Romp E, Czapka A, Rao Z, Kretzer C, Koeberle A, Garscha U, Pace
1201 S, Claesson H, *et al* (2019) Targeting biosynthetic networks of the proinflammatory and
1202 proresolving lipid metabolome. *FASEB J* 33: 6140–6153
1203 Werz O, Gerstmeier J, Libreros S, Rosa XD la, Werner M, Norris PC, Chiang N & Serhan CN
1204 (2018) Human macrophages differentially produce specific resolvin or leukotriene signals
1205 that depend on bacterial pathogenicity. *Nat Commun* 9: 59
1206 Wilcock DJ, Badrock AP, Wong CW, Owen R, Guerin M, Southam AD, Johnston H, Telfer BA,
1207 Fullwood P, Watson J, et al (2022) Oxidative stress from DGAT1 oncoprotein inhibition in
1208 melanoma suppresses tumor growth when ROS defenses are also breached. *Cell Reports*
1209 39: 110995
1210 Wooten RE, Willingham MC, Daniel LW, Leslie CC, Rogers LC, Sergeant S & O'Flaherty JT
1211 (2008) Novel translocation responses of cytosolic phospholipase $A_2\alpha$ fluorescent proteins.
1212 *Biochim Biophys Acta* 1783: 1544–1550
1213 Yin H, Li W, Mo L, Deng S, Lin W, Ma C, Luo Z, Luo C & Hong H (2021) Adipose triglyceride
1214 lipase promotes the proliferation of colorectal cancer cells via enhancing the lipolytic
1215 pathway. *J Cell Mol Med* 25: 3963–3975
1216 Zagani R, El-Assaad W, Gamache I & Teodoro JG (2015) Inhibition of adipose triglyceride
1217 lipase (ATGL) by the putative tumor suppressor G0S2 or a small molecule inhibitor
1218 attenuates the growth of cancer cells. *Oncotarget* 6: 28282–28295
1219 Zechner R, Madeo F & Kratky D (2017) Cytosolic lipolysis and lipophagy: two sides of the
1220 same coin. *Nat Rev Mol Cell Biol* 18: 671–684
1221 Zechner R, Zimmermann R, Eichmann TO, Kohlwein SD, Haemmerle G, Lass A & Madeo F
1222 (2012) FAT SIGNALS - Lipases and lipolysis in lipid metabolism and signaling. *Cell Metab*
1223 15: 279–291
1224 Zimmermann R, Strauss JG, Haemmerle G, Schoiswohl G, Birner-Gruenberger R, Riederer
1225 M, Lass A, Neuberger G, Eisenhaber F, Hermetter A, *et al* (2004) Fat mobilization in
1226 adipose tissue is promoted by adipose triglyceride lipase. *Science* 306: 1383–1386
1227 Zoni V, Khaddaj R, Campomanes P, Thiam AR, Schneiter R & Vanni S (2021) Pre-existing
1228 bilayer stresses modulate triglyceride accumulation in the ER *versus* lipid droplets. *Elife*
1229 10: e62886
1230
1231
1232

Figures and figure legends

Figure 1

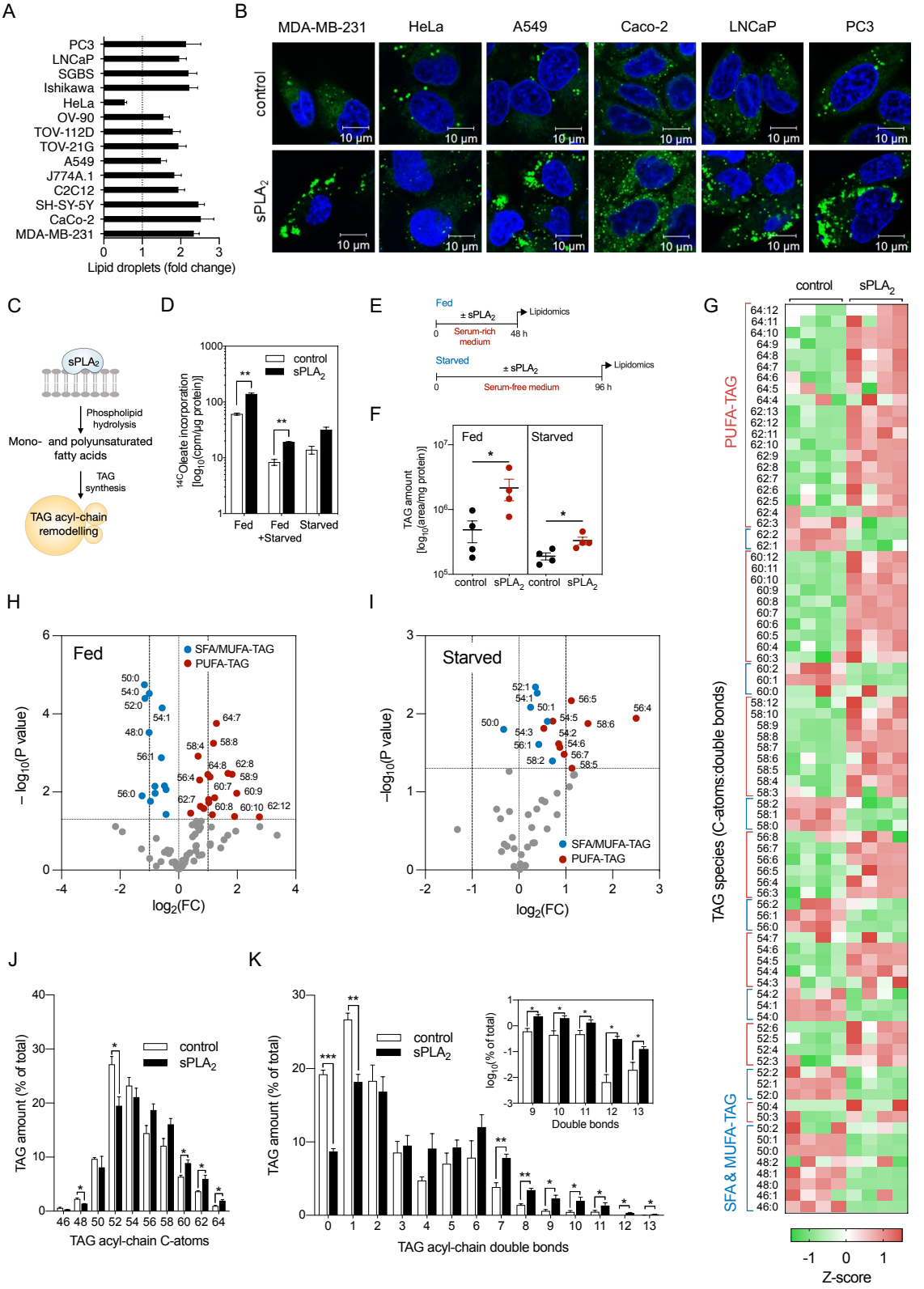

Figure 1. sPLA2 promotes enrichment of LDs with long-chain PUFA-containing triglycerides. (**A, B**) LD levels in control cells and cells treated with 10 nM recombinant hGX sPLA2 for 48 h in serum-rich

medium. (**A**) Neutral lipid content was quantified by Nile Red staining and flow cytometry (n = 3 independent experiments; 20000 cells per treatment). (**B**) Representative live-cell confocal microscopy images of LDs stained with BODIPY 493/503 (green) and nuclei with Hoechst 33342 (blue). (**C**) Diagram illustrating the hypothesis that unsaturated fatty acids released through $sPLA_2$ membrane hydrolysis are incorporated into triacylglycerols (TAGs) and lead to lasting changes in LD TAG acyl-chain composition. (**D**) hGX-$sPLA_2$-induced changes in the incorporation of radiolabelled oleate into cellular TAGs in MDA-MB-231 cells grown in complete medium for 24 h (Fed), in complete medium for 24 h followed by 96 h of serum starvation (Fed + Starved), and in serum-free medium for 96 h (Starved) (n = 4 independent experiments). (**E**) Diagram illustrating the experimental treatments used for lipidomic analysis in (F)–(K). (**F–K**) TAG lipidomic analyses of MDA-MB-231 cells treated with recombinant hGX $sPLA_2$ in complete medium for 48 h (Fed; F–H, J, K) or in the absence of serum for 96 h (Starved; F, I). Cell lysates were collected and analysed by UPLC/qTOF-MS (n = 4 independent experiments). (**G–I**) $sPLA_2$-induced changes in the levels of individual TAG species presented as a representative *z*-score heat-map (G) and volcano plots (H, I) prepared by log_2 data transformation and multiple t-test analyses (n = 4 independent experiments). Statistically significant changes ($-log_{10}$(P value) > 1.30) in TAGs containing mostly saturated and mono-unsaturated FAs (SFA/MUFA-TAGs with 0–2 double bonds; blue) and those containing polyunsaturated FAs (PUFA-TAGs with 3–12 double bonds; red) are shown. (**J, K**) $sPLA_2$-induced changes in relative levels of TAG species grouped by number of acyl-chain C-atoms (chain length) and double bonds (chain unsaturation). (A–K) Data are means ±SEM of at least three independent experiments. *, P <0.05; **, P <0.01; ***, P <0.001 (unpaired t-tests).

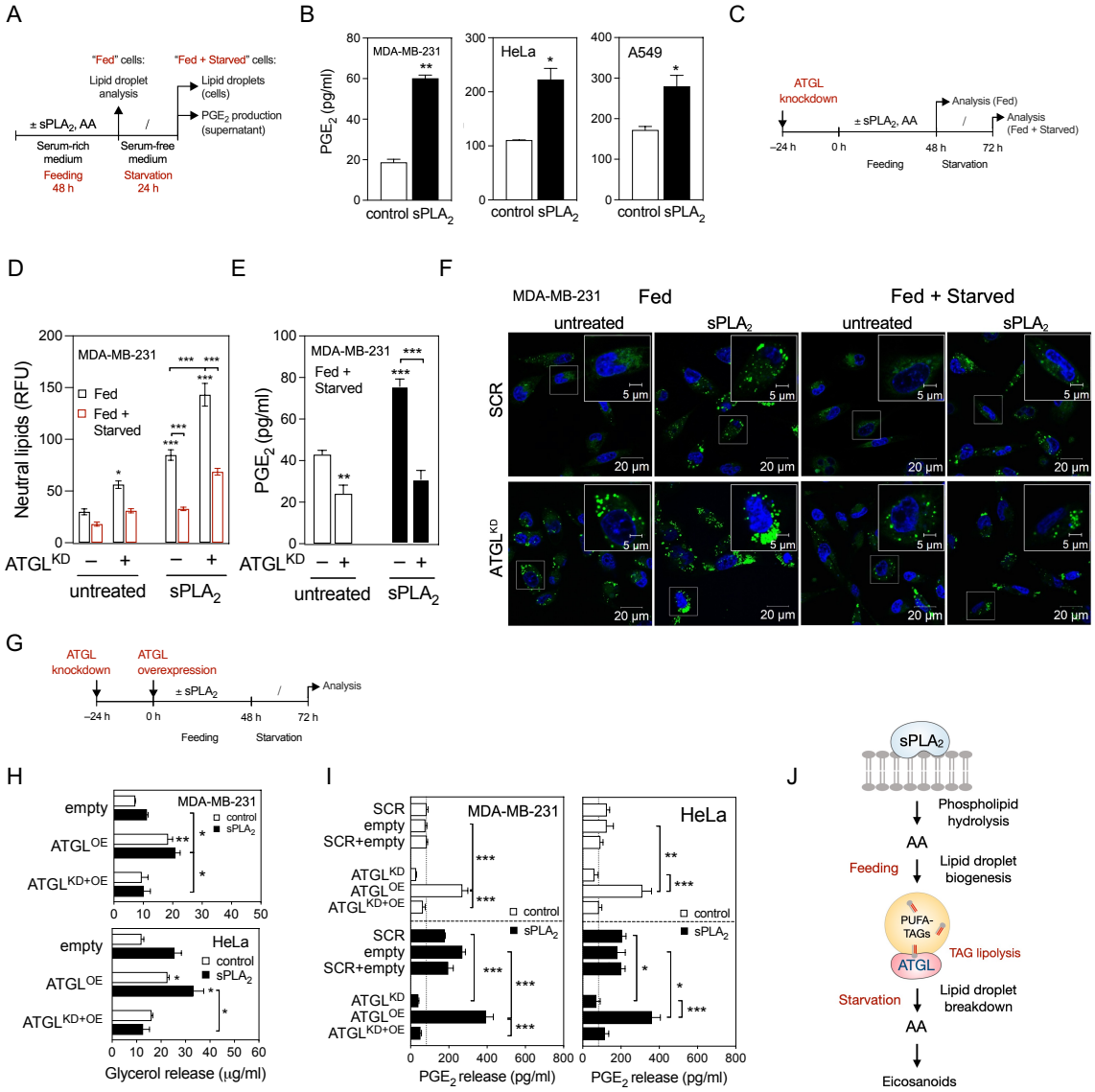

Figure 2. ATGL-mediated LD breakdown is required for PGE_2 production in serum-starved cancer cells. (**A**) Diagram illustrating the experimental set-up used to load cells with LDs (Feeding) and then to induce their breakdown (Starvation). (**B**) PGE_2 levels in cell supernatants of control and hGX-$sPLA_2$-treated cells quantified by ELISA at the end of the starvation period. (**C**) Diagram illustrating the experimental conditions used in (D)–(F) and Supp. Fig. 1(E)–(O). (**D, E**) LD levels and PGE_2 production in ATGL-silenced control and $sPLA_2$-treated cells grown as shown in (C) and analysed at the beginning (Fed) and at the end of the serum starvation period (Fed + Starved). Neutral lipids were quantified by Nile Red staining and flow cytometry, PGE_2 was quantified by ELISA. (**F**) Representative confocal microscopy images showing effects of ATGL depletion on cellular LD content in control and hGX-$sPLA_2$-treated cells, under serum-rich (Fed) and serum-free (Fed + Starved) conditions. LDs and nuclei were

stained using BODIPY 493/503 and Hoechst 33342, respectively. (**G**) Diagram illustrating the experimental set-up used in (H), (I) and Supp. Figure 1P, R. (**H, I**) Glycerol release and PGE_2 production in ATGL-overexpressing serum-starved cells (both untreated and hGX $sPLA_2$ pretreated), in comparison with cells co-transfected with ATGL-specific siRNAs ($ATGL^{KD+OE}$), non-targeting siRNA (scrambled) and control plasmid (empty), grown as illustrated in (G). (**J**) Diagram illustrating the proposed model of LD-mediated eicosanoid production in cancer cells. Data are means ±SEM of two (H) or three (B–E, I) independent experiments. *, P <0.05; **, P <0.01; ***, P <0.001 (two-way ANOVA with Tukey (I) or Bonferroni (D, E, H) adjustment; unpaired t-tests (B)).

Figure 3

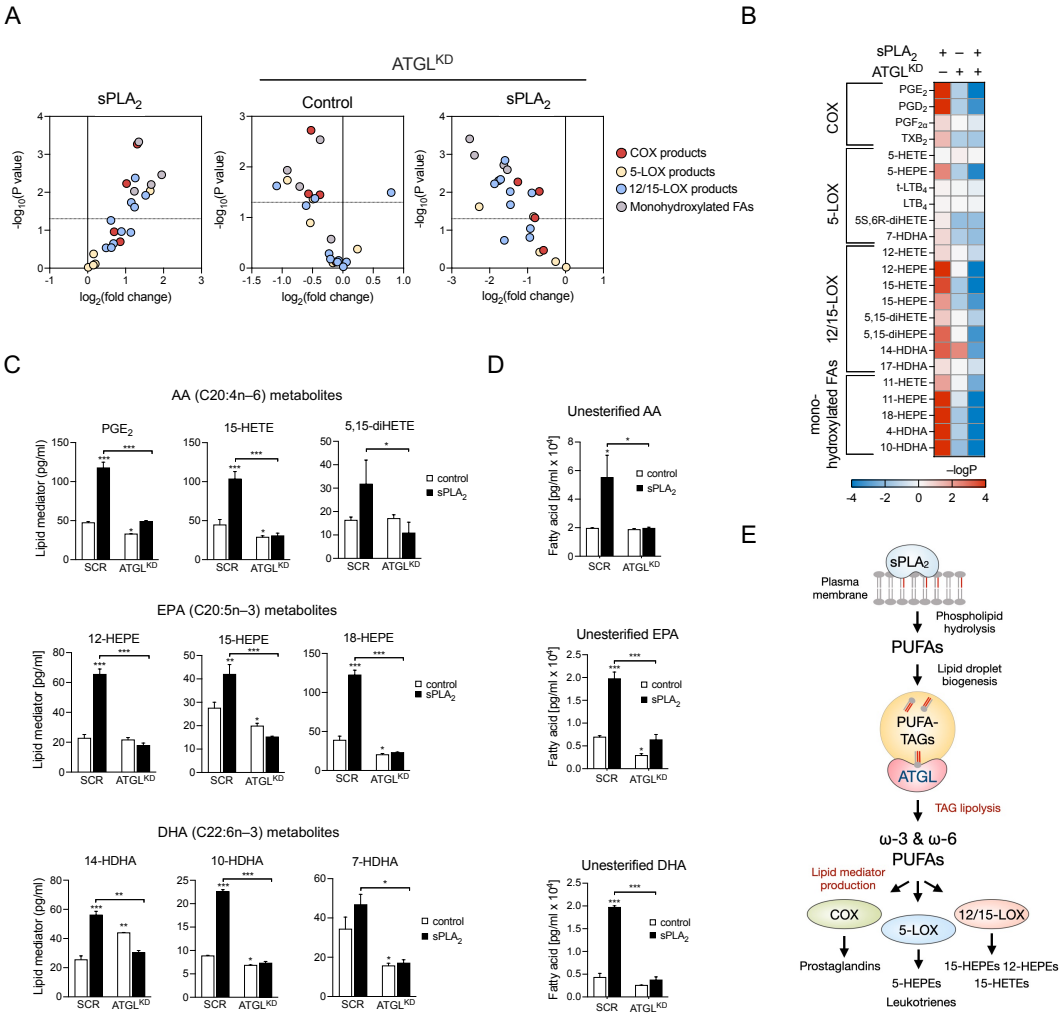

Figure 3. ATGL-mediated lipolysis drives production of a wide spectrum of bioactive lipid mediators. (**A–D**) UPLC-MS-MS analysis of lipid mediators released from serum-starved MDA-MB-231 cells pre-treated with hGX $sPLA_2$, and from ATGL-depleted cells without and with hGX $sPLA_2$ pre-treatment, presented as volcano plots (A), a heat map (B), and individual graphs (C, D). Cells were treated as shown in Fig. 2C. Volcano plots were prepared using log_2-transformed fold-change values and multiple t-test analysis, and the heat map by –logP data transformation and two-way ANOVA with

1298 Sidak adjustment (n = 3 independent experiments). (**E**) Diagram illustrating the involvement of hGX
1299 $sPLA_2$ and ATGL in the production of a wide range of PUFA-derived cyclooxygenase (COX) and
1300 lipoxygenase (LOX) signalling molecules. Data are means ±SEM of three independent experiments. *,
1301 P <0.05; **, P <0.01; ***, P <0.001 (two-way ANOVA with Sidak adjustment).

Figure 4

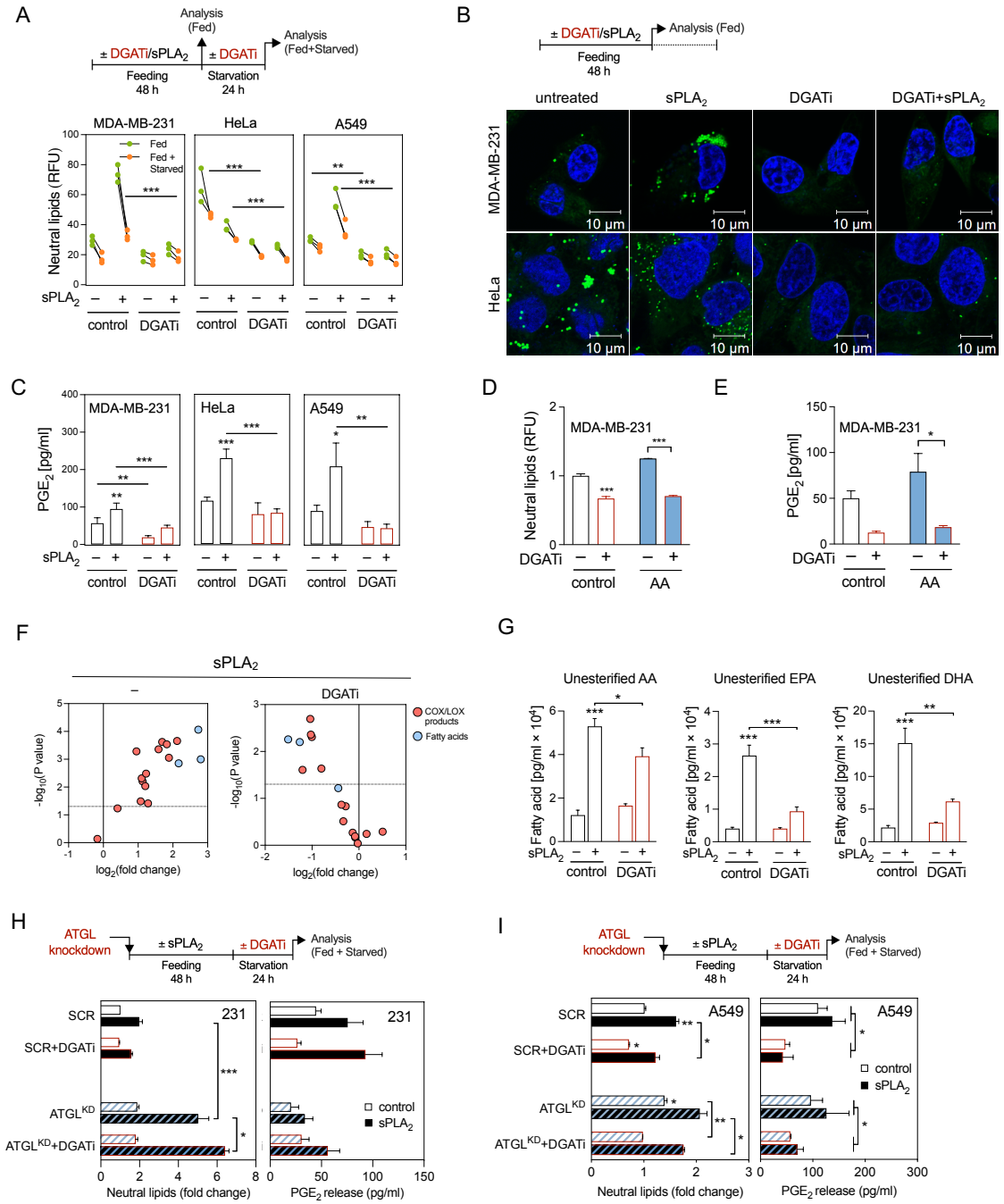

1302

1303 **Figure 4. DGAT-mediated LD biogenesis is required for lipid mediator production in serum-**
1304 **starved cancer cells.** (**A**) Diagram illustrating the experimental conditions used (top) and cellular
1305 neutral lipid content before (Fed) and after (Fed + Starved) serum starvation in cells treated with DGAT1
1306 (T863) and DGAT2 (PF-06427878) inhibitors (DGATi), without and with stimulation of LD biogenesis by
1307 hGX $sPLA_2$ during serum sufficiency. (**B**) Representative confocal microscopy images of live cells under

1308 nutrient-replete conditions and treated with DGAT inhibitors in the absence and presence of hGX $sPLA_2$.
1309 LDs and nuclei were visualised using BODIPY 493/503 and Hoechst 33342 staining, respectively, and
1310 confocal microscopy. (**C**) DGATi-induced changes in PGE_2 production in serum-starved cancer cells
1311 (Fed + Starved), without and with additional stimulation of LD biogenesis by hGX $sPLA_2$ pre-treatment.
1312 Cells were treated according to (A). (**D, E**) DGATi-induced changes in neutral lipids (D) and PGE_2
1313 production (E) in serum-starved MDA-MB-231 cancer cells (Fed + Starved), without and with additional
1314 stimulation of LD biogenesis by arachidonic acid (AA) pre-treatment. Cells were treated according to
1315 (A). (**F, G**) DGATi-induced changes in the profiles of lipid mediators and fatty acids released from serum-
1316 starved MDA-MB-231 cells treated with hGX $sPLA_2$, without and with treatment with an equimolar mix
1317 of DGAT1 and DGAT2 inhibitors according to (A). Volcano plots (F) show significant changes ($-\log_{10}$(P
1318 value) >1.30) in individual lipids between hGX $sPLA_2$-treated *versus* control cells (left) and hGX $sPLA_2$-
1319 treated *versus* hGX $sPLA_2$- and DGATi-treated (right) cells and were prepared using $\log_2$-transformed
1320 fold-change values and multiple t-test analysis (n = 4 independent experiments). (**H, I**) Diagrams
1321 illustrating the experimental conditions used (top) and changes in PGE_2 production induced by DGATi
1322 treatments during serum starvation in control (SCR) and ATGL-depleted ($ATGL^{KD}$) MDA-MB-231 (H)
1323 and A549 (I) cells, without and with hGX $sPLA_2$ pre-treatment. (A, D, H, I) Neutral lipid content was
1324 quantified by Nile Red staining and flow cytometry. (C, E, H, I) PGE_2 levels were determined in cell
1325 supernatants as described in Methods. (F, G) UPLC-MS/MS analysis of lipid mediators and FAs in cell
1326 supernatants was performed as described in Methods. Data are means ±SEM of at least three (A, C, D,
1327 E, H, I) or four (F, G) independent experiments. *, P <0.05; **, P <0.01; ***, P <0.001 (two-way ANOVA
1328 with Tukey (A, H, G, I) or Bonferroni (C, D, E) adjustment).

Figure 5

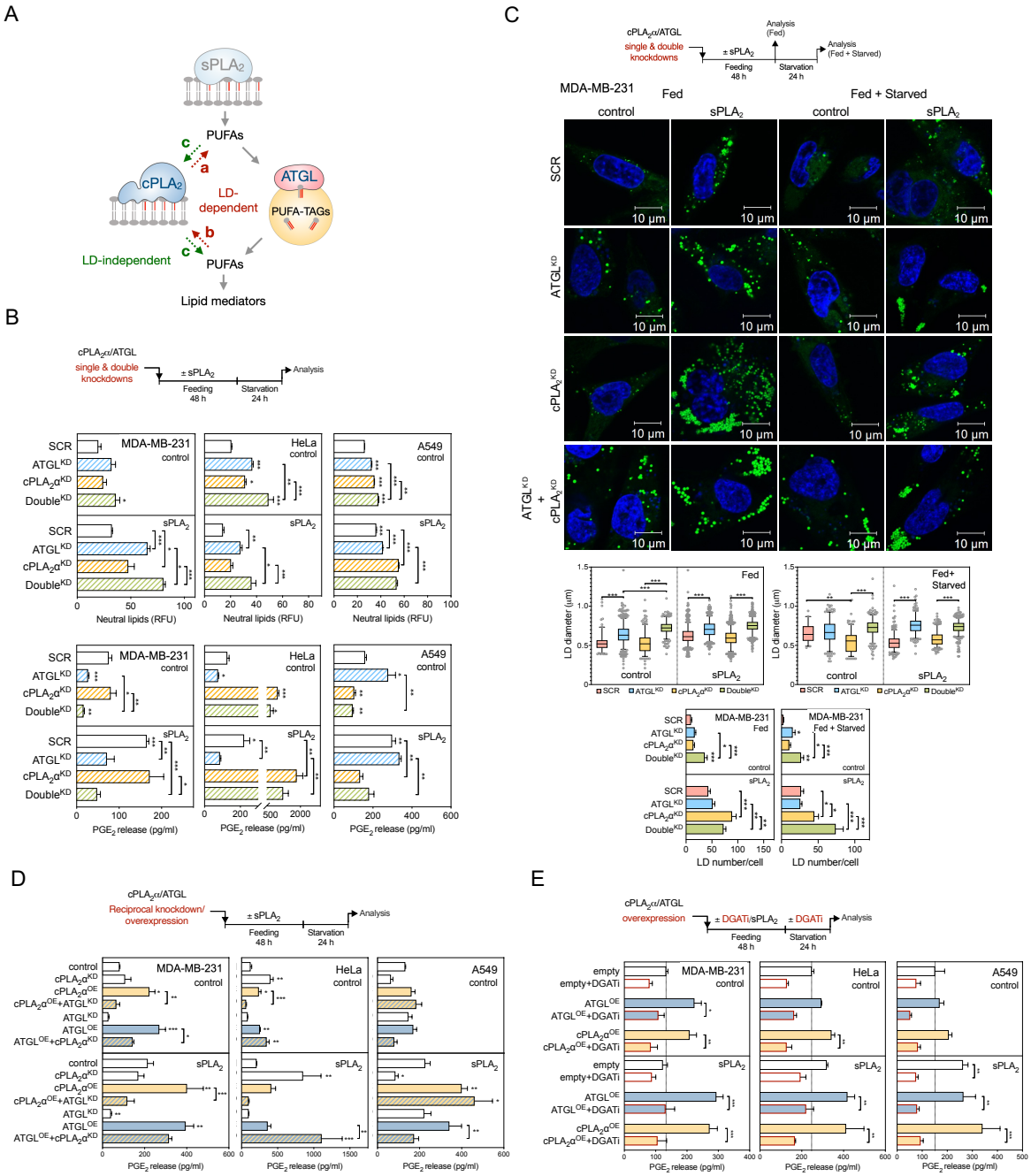

Figure 5. cPLA₂α depends on LD turnover to drive lipid mediator production. (**A**) Scheme illustrating hypothetical models of interplay between cPLA₂α and LDs in providing PUFAs for lipid mediator production. (**B**) Changes in neutral lipid content and PGE_2 production induced by ATGL ($ATGL^{KD}$) and cPLA₂α ($cPLA_2\alpha^{KD}$) single and double ($Double^{KD}$) knockdowns, in comparison with control siRNA-treated cells (SCR), without and with stimulation of LD biogenesis by hGX $sPLA_2$ pre-treatment. (**C**) Diagram illustrating the experimental conditions used (top), representative live-cell confocal microscopy images (middle) and image analysis (bottom) of LDs in ATGL ($ATGL^{KD}$) and cPLA₂α ($cPLA_2\alpha^{KD}$) single and double ($Double^{KD}$) knockdown MDA-MB-231 cells, in comparison with non-targeting control siRNA-treated cells (SCR), without and with stimulation of LD biogenesis by hGX $sPLA_2$ pre-treatment. LDs were stained with BODIPY 493/503 (green) and nuclei with Hoechst 33342 (blue)

1340 and images analysed using ImageJ and the LD Counter Plugin. Box plots are showing changes in LD
1341 diameters and bar plots changes in LD numbers per cell in serum-fed (Fed) and serum-starved (Starved)
1342 cells. Data are geometric means (diameter analysis) or means (number analysis) ±SEM (n >40
1343 cells/sample) of two independent experiments. (**D**) PGE_2 production in cells with reciprocal
1344 knockdown/overexpression of $cPLA_2\alpha$ and ATGL. Cells were reverse transfected with siRNAs specific
1345 for ATGL ($ATGL^{KD}$) and/or $cPLA_2\alpha$ ($cPLA_2\alpha^{KD}$), then forward transfected with ATGL-encoding ($ATGL^{OE}$)
1346 and/or $cPLA_2\alpha$-encoding ($cPLA_2\alpha^{OE}$) plasmids, without and with pre-treated with hGX $sPLA_2$, as
1347 illustrated in the scheme (top). In controls (control), non-targeting siRNA reverse transfections were
1348 combined with backbone ('empty') vector forward transfections. (**E**) DGAT inhibition (DGATi)-induced
1349 changes in PGE_2 production in serum-starved control cells (empty) and in cells overexpressing ATGL
1350 ($ATGL^{OE}$) or $cPLA_2\alpha$ ($cPLA_2\alpha^{OE}$), without and with additional stimulation of LD biogenesis by hGX $sPLA_2$
1351 pre-treatment. Neutral lipid content was quantified by Nile Red staining and flow cytometry (B), PGE_2
1352 levels were determined in cell supernatants using ELISA (B, D, E). Data are means ±SEM of two (B,
1353 A549 cells) or at least three independent experiments *, P <0.05; **, P <0.01; ***, P <0.001 (nested one-
1354 way ANOVA with Sidak adjustment (C, box plots), two-way ANOVA with Tukey (B, C, E) or Dunnet (D)
1355 adjustment).

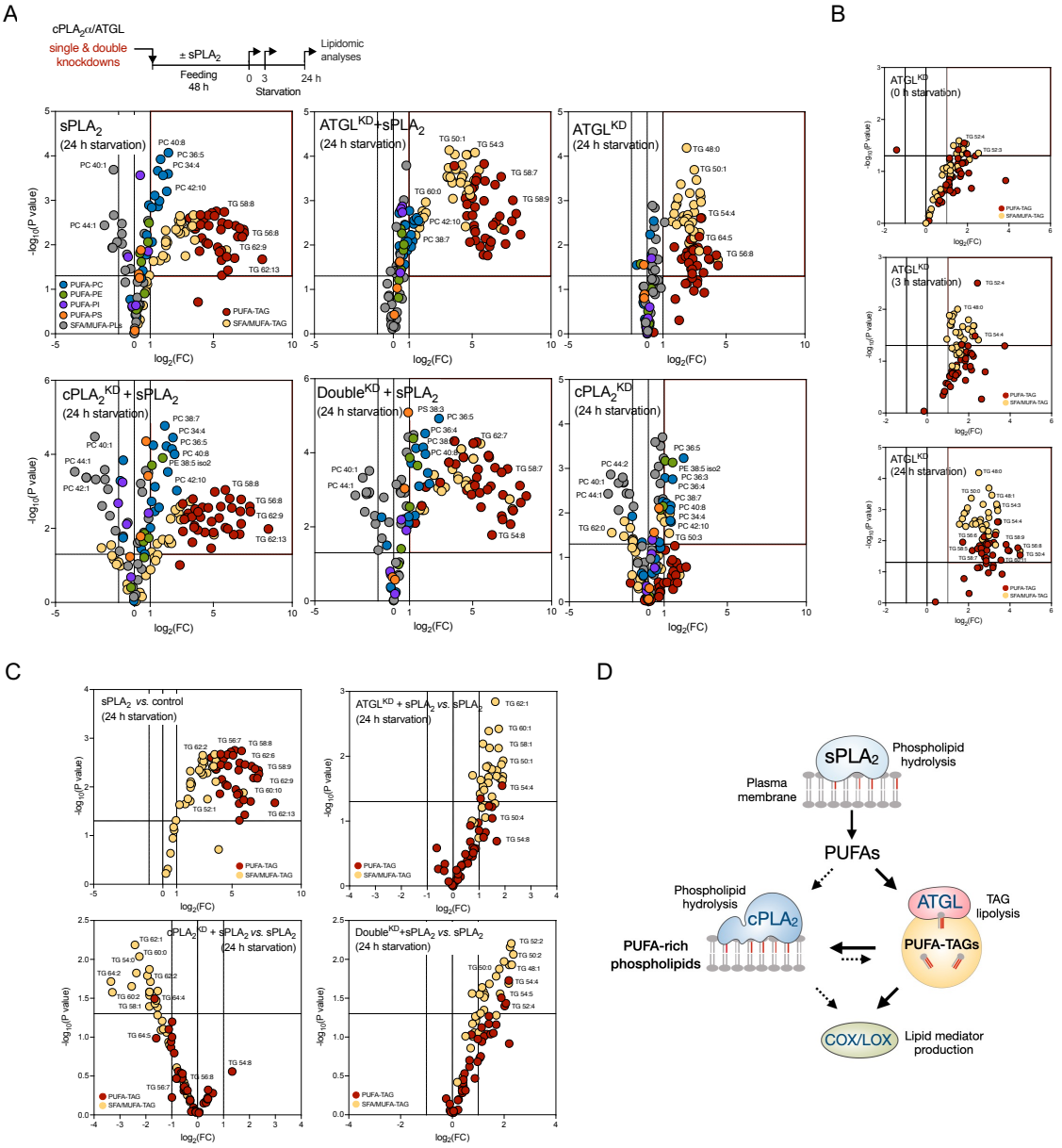

Figure 6. ATGL and cPLA$_2$α cooperatively modulate PUFA trafficking between triglycerides and membrane phospholipids. (**A–C**) Untargeted lipidomic analysis of phospholipids and triglycerides (TAGs) in serum-starved MDA-MB-231 cells depleted of ATGL (ATGL^{KD}), cPLA$_2$α (cPLA$_2$α^{KD}), or both (Double^{KD}), without and with hGX sPLA$_2$ pre-treatment under serum-rich conditions, and grown as shown in the diagram (A). Volcano plots show significant changes (–log$_{10}$(P value) >1.30) in individual lipids between each treatment condition *versus* control cells (unless otherwise indicated), and were prepared by log$_2$ fold-change (FC) data transformation and multiple t-test analysis (n=3 independent experiments). TAGs and phospholipids (PLs) containing saturated and mono-unsaturated acyl chains

(SFA/MUFA-TAGs, SFA/MUFA-PLs, with 0–3 and 0–2 double bonds, respectively) and those containing polyunsaturated FAs (PUFA-TAGs, PUFA-PLs, with at least 4 and 3 double bonds, respectively) are colour-coded as indicated. TG, triglyceride; PC, phosphatidylcholine; PE, phosphatidylethanolamine; PI, phosphatidylinositol, PS, phosphatidylserine. (**D**) Schematic illustration of the predominant pathways involved in LD-mediated PUFA trafficking between the membrane phospholipid and TAG pools in serum-starved cancer cells.

Figure 7

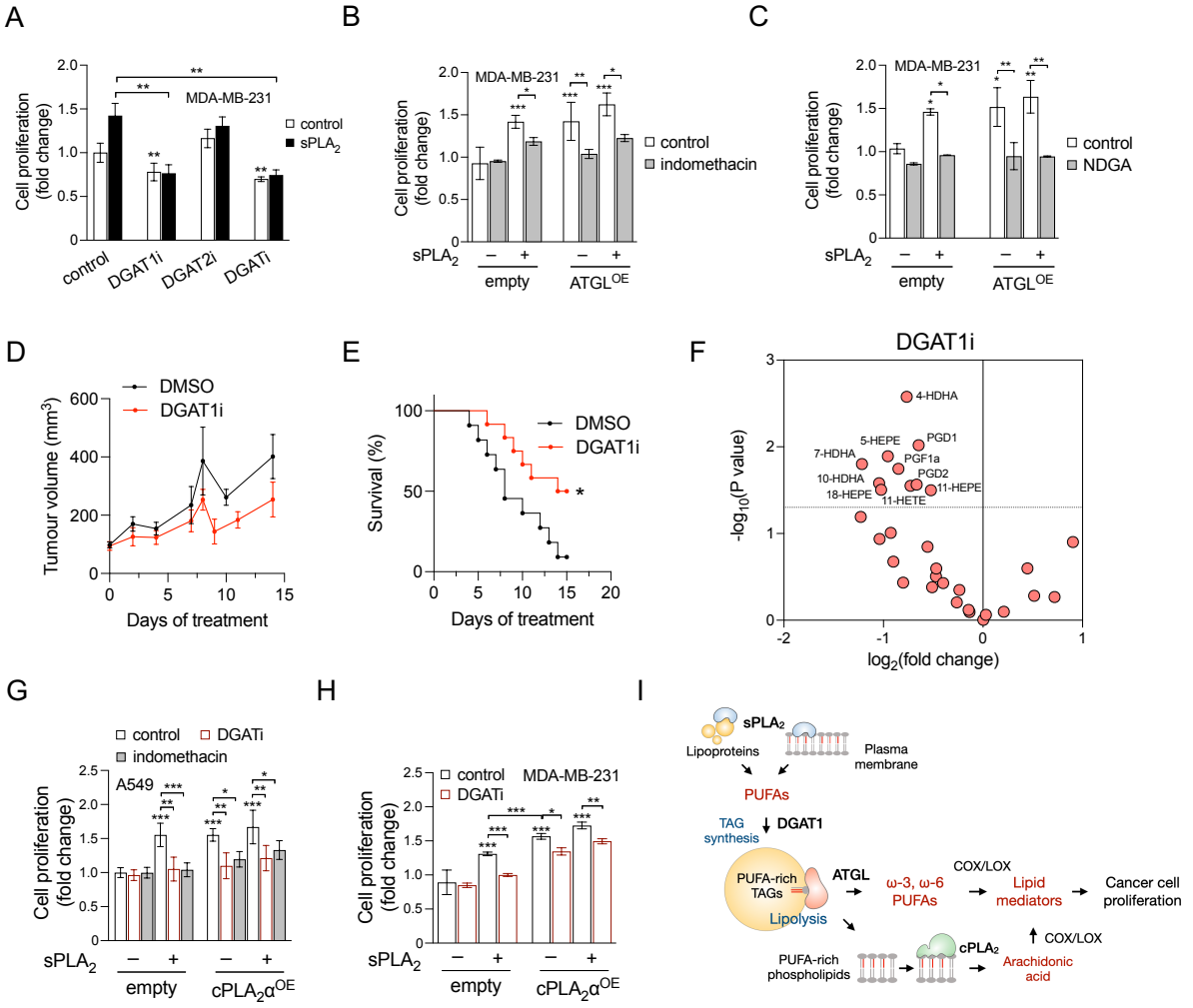

Figure 7. LD-mediated lipid mediator production promotes cancer-cell proliferation and tumor growth. (**A**) Proliferation of MDA-MB-231 cells treated with T863 (DGAT1i) and PF-06427878 (DGAT2i), or an equimolar mix of both DGAT inhibitors (DGATi), grown under nutrient-rich conditions in the absence and presence of hGX sPLA$_2$. (**B, C**) Proliferation of MDA-MB-231 cells overexpressing ATGL (ATGL^{OE}), treated with indomethacin (B) or nordihydroguaiaretic acid (NDGA) (C), in the absence and presence of hGX sPLA$_2$. (**D**, **E**) Tumour growth (D) and corresponding Kaplan-Meier survival curves (E) of mice bearing MDA-MB-231 xenografts and treated daily with the DGAT1 inhibitor T863 or with 0.2% DMSO vehicle. Significance was determined by log-rank (Mantel-Cox) test (**F**) DGAT1-inhibitor-induced changes in the abundance of lipid mediators and PUFAs in tumour samples isolated from mice bearing

1381 MDA-MB-231 xenografts and treated daily with DGAT1 inhibitor T863 or with 0.2% DMSO vehicle. The
1382 volcano plot depicts significant changes ($-\log_{10}$(P value) >1.30) in individual lipids detected by UPLC-
1383 MS/MS in DGAT1i-treated *versus* vehicle-treated mice and was prepared using $\log_2$-transformed fold-
1384 change values and multiple t-test analysis (n = 4 independent experiments). (**G**) Proliferation of A549
1385 cells overexpressing $cPLA_2\alpha$ ($cPLA_2\alpha^{OE}$) and grown in the absence and presence of DGATi,
1386 indomethacin and recombinant hGX $sPLA_2$. (**H**) Proliferation of MDA-MB-231 cells overexpressing
1387 $cPLA_2\alpha$ ($cPLA_2\alpha^{OE}$) and grown in the absence and presence of DGATi and recombinant hGX $sPLA_2$.
1388 Data are means ±SEM of three independent experiments. *, P <0.05; **, P <0.01; ***, P <0.001 (two-
1389 way ANOVA with Tukey (A), Bonferroni (B, C) or Sidak (G, H) adjustments).
1390
1391
1392

Supplementary Material

Manuscript title:

Lipid droplets control mitogenic lipid mediator production in human cancer cells

Authors:

Eva Jarc Jovičić[1,2], Anja Pucer Janež[1,2], Thomas O. Eichmann[3,4], Špela Koren[1,2], Vesna Brglez[1,2], Paul M. Jordan[5], Jana Gerstmeier[5], Duško Lainšček[6,7], Anja Golob-Urbanc[6], Roman Jerala[6,7], Gérard Lambeau[8], Oliver Werz[5], Robert Zimmermann[3,9], and Toni Petan[1,*]

Contents:

Supplementary Figures and Supplementary Figure Legends

Supp. Fig. 1

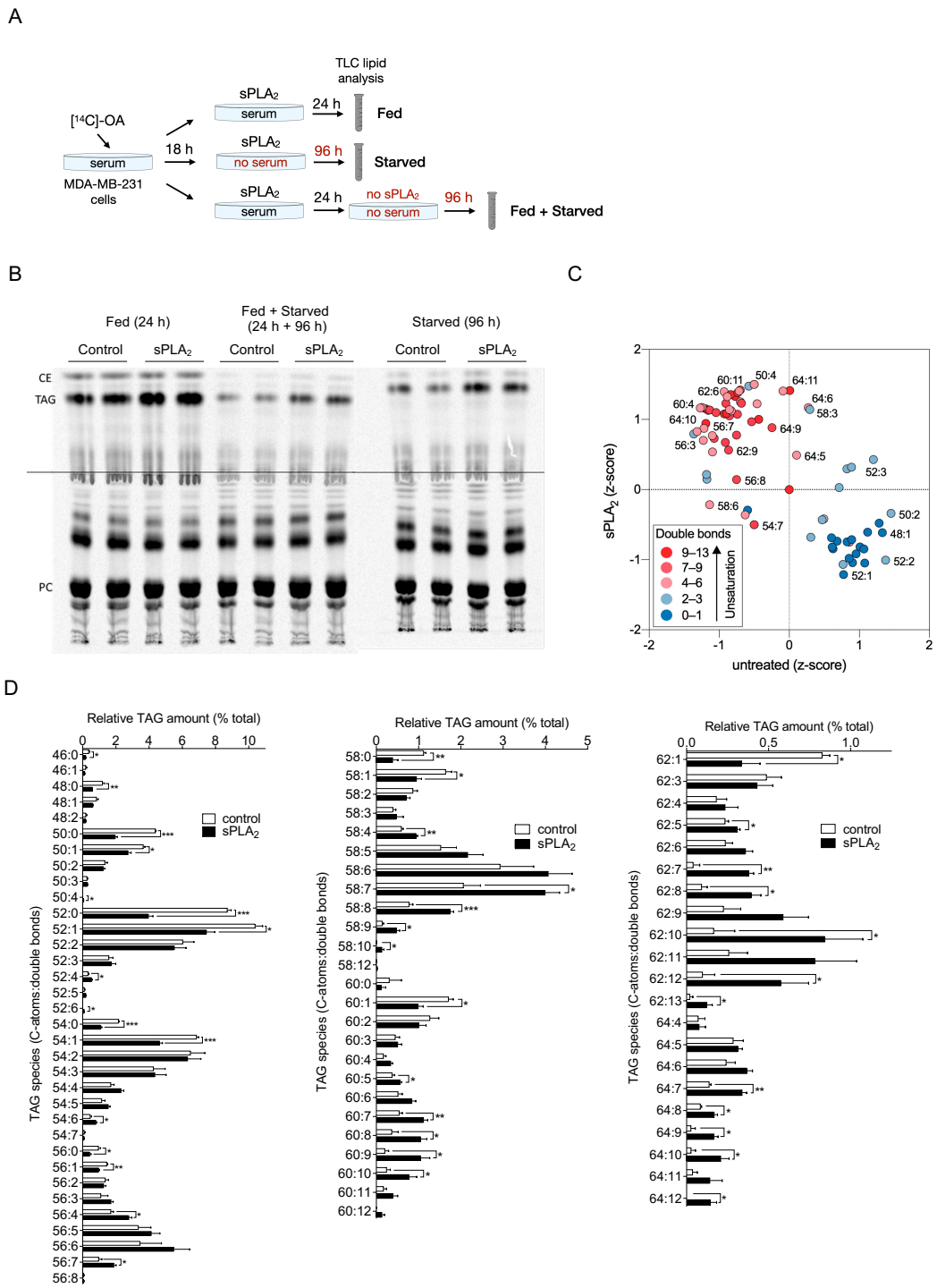

Supplementary Figure 1. sPLA$_2$-induced changes in LD metabolism and composition. (**A, B**) Diagram illustrating the experimental set-up for oleate incorporation analyses shown in (B) and in Figure 1D. (B) Representative thin layer chromatography (TLC) plate showing that in hGX-sPLA$_2$-treated cells, oleate is preferentially incorporated into TAGs, but not into phosphatidylcholine (PC) or cholesterol esters (CE). (**C, D**) Lipidomic analysis of hGX-sPLA$_2$-induced PUFA-TAG enrichment in MDA-MB-231 cells grown under serum-rich conditions. (C) Representative XY z-score plot showing colour-coded

39 changes in the levels of TAG acyl-chain unsaturation. Data are means ±SEM of three or four (D)
40 independent experiments. *, P <0.05; **, P <0.01; ***, P <0.001 (unpaired t-tests (D).
41
42

Supp. Fig. 2

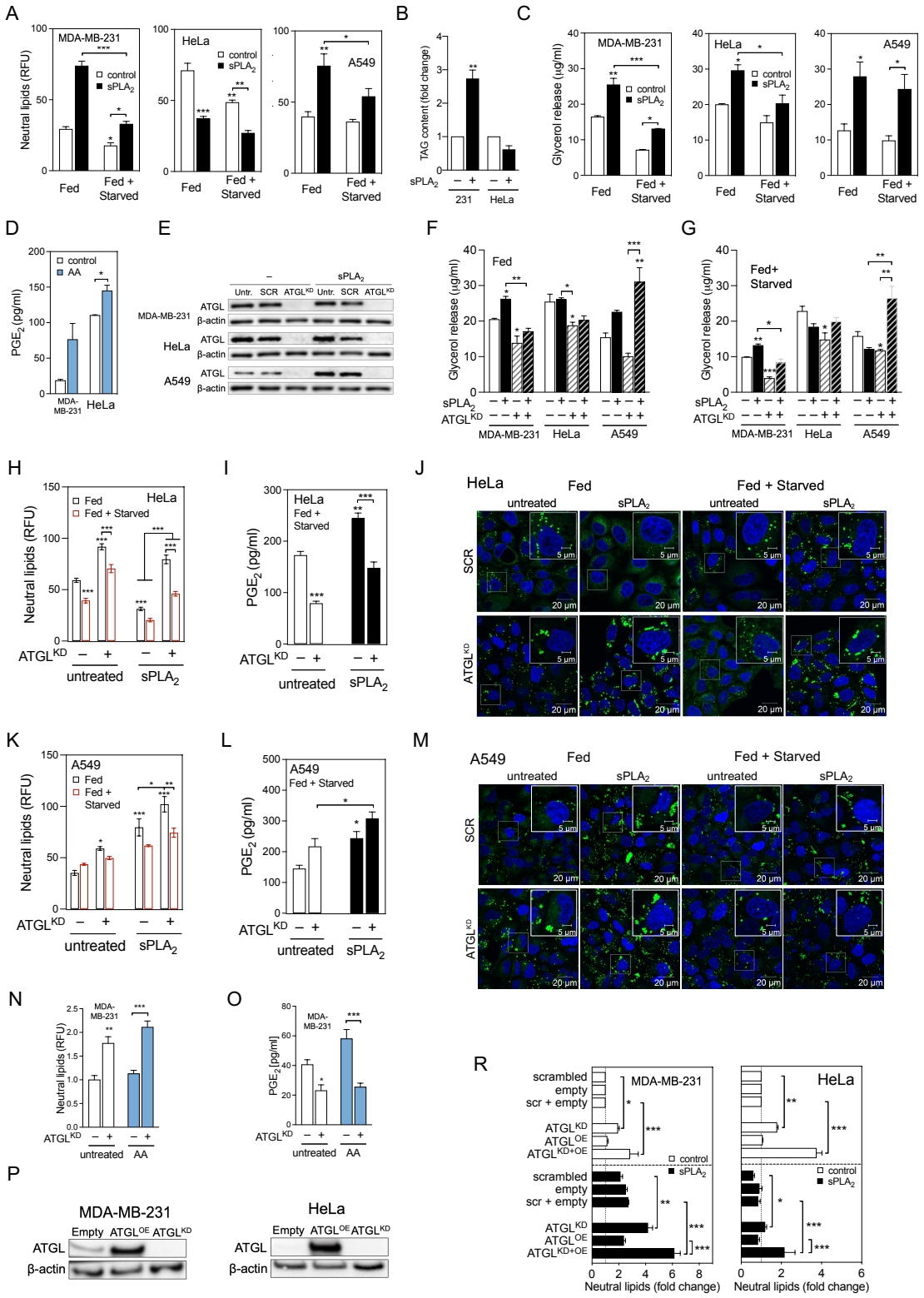

Supplementary Figure 2. ATGL-mediated LD breakdown drives PGE_2 production in starving MDA-MB-231 and HeLa cells, but not in A549 cells. (**A**) Neutral lipid contents in control and hGX-$sPLA_2$-treated cells at the beginning of and after serum starvation. (**B**) Total cellular triglycerides (TAGs) in control and hGX-$sPLA_2$-treated MDA-MB-231 and HeLa cells quantified using a biochemical assay. (**C**) Glycerol released from fed and starving control and hGX-$sPLA_2$-treated cells. (**D**) PGE_2 levels in cell supernatants of control and AA-treated cells. (**E**) Representative western blot showing siRNA-induced ATGL knock down ($ATGL^{KD}$) in comparison with control (untransfected [untr.] and non-targeting siRNA-transfected [SCR] cells), treated and grown as shown in Fig. 2C. (**F, G**) Glycerol released in cell supernatants of control and ATGL-depleted serum-fed and serum-starved cells, either untreated or treated with hGX $sPLA_2$. (**H, I, K, L**) Neutral lipid and PGE_2 levels in ATGL-silenced control and $sPLA_2$-treated cells grown and analysed as shown in Fig. 2C. (**J, M**) Representative confocal microscopy images showing effects of ATGL depletion on cellular LD content in control and hGX-$sPLA_2$-treated cells, under serum-rich (Fed) and serum-free (Fed + Starved) conditions. LDs and nuclei were stained using BODIPY 493/503 and Hoechst 33342, respectively. (**N, O**) Changes in LD levels and PGE_2 production induced by ATGL silencing in control and arachidonic acid (AA)-treated cells analysed as shown in Fig. 2C. (**P**) Representative western blot showing ATGL protein overexpression in cells transfected with ATGL-encoding plasmid ($ATGL^{OE}$) in comparison with those transfected with control (Empty) vector or ATGL-specific siRNA ($ATGL^{KD}$), grown as illustrated in Fig. 2G. (**R**) Neutral lipid levels in ATGL-overexpressing in untreated and hGX-$sPLA_2$-pretreated serum-starved cells, in comparison with those co-transfected with ATGL-specific siRNA ($ATGL^{KD+OE}$), non-targeting siRNA (scrambled) and control plasmid (empty), grown as shown in Fig. 2G. (A, H, K, N, R) Neutral lipids were quantified by Nile Red staining and flow cytometry. (D, I, L, O) PGE_2 was quantified by ELISA at the end of starvation. Data are means ±SEM of two (D) or three (A–C, F–I, K, L, N, O) independent experiments. *, $P < 0.05$; **, $P < 0.01$; ***, $P < 0.001$ (two-way ANOVA with Bonferroni (B, F–I, K, L, N, O) or Tukey (A, C, R) adjustment; unpaired t-test (D)).

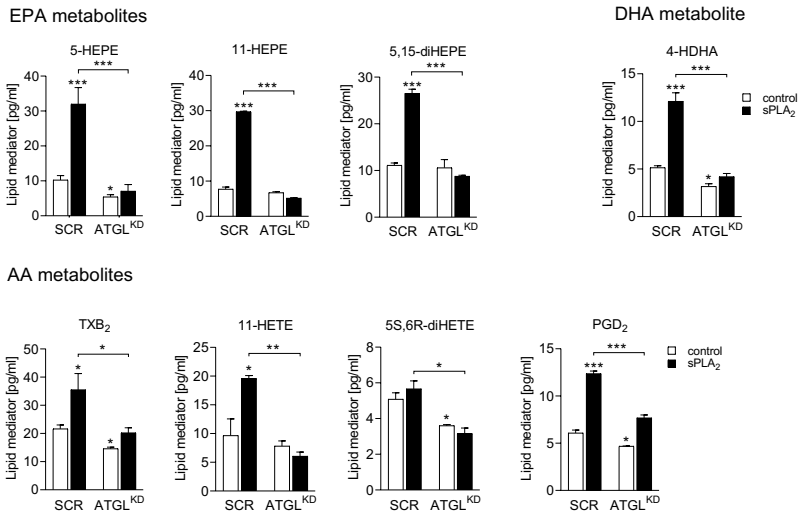

Supplementary Figure 3. Depletion of ATGL suppresses both basal and hGX-sPLA$_2$-stimulated lipid mediator production in breast cancer cells. hGX-sPLA$_2$-induced and ATGL knockdown (ATGL^{KD})-induced changes in selected lipid mediators (as indicated) released from serum-starved MDA-MB-231 cells. Data are means ±SEM of three independent experiments. *, P <0.05; **, P <0.01; ***, P <0.001 (two-way ANOVA with Sidak adjustment). DHA, docosahexaenoic acid; 4-HDHA, 4-hydroxydocosahexaenoic acid; EPA, eicosapentaenoic acid; HEPE, hydroxyeicosapentaenoic acid; HETE, hydroxyeicosatetraenoic acid; AA, arachidonic acid; TXB$_2$, thromboxane B$_2$.

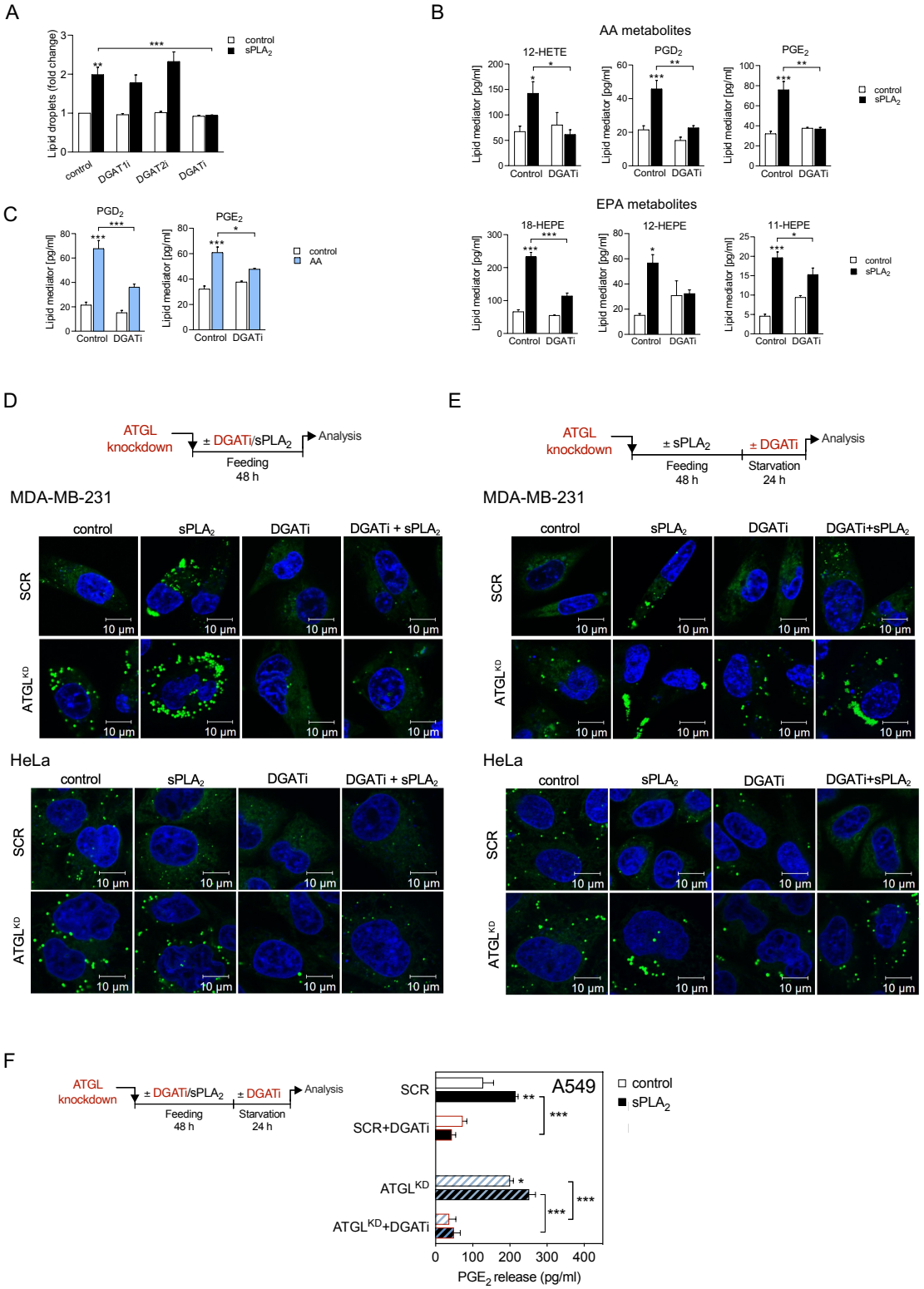

Supplementary Figure 4. Lipid mediator production induced by hGX sPLA2 or exogenous AA depends on DGAT-mediated LD biogenesis. (**A**) Neutral lipid content in MDA-MB-231 cells grown in the absence and presence of T863 (DGAT1i) and PF-06427878 (DGAT2i), or an equimolar mix of both

83 DGAT inhibitors (DGATi), without and with stimulation of LD biogenesis by hGX $sPLA_2$ during serum
84 sufficiency. (**B**) hGX-$sPLA_2$-induced and DGAT inhibition (DGATi)-induced changes in selected lipid
85 mediators (as indicated) released from serum-starved MDA-MB-231 cells. Cells were treated as shown
86 in Figure 4A. (**C**) AA-induced and DGATi-induced changes in selected lipid mediators (as indicated).
87 Cells were treated as shown in Figure 4A. (**D, E**) Diagrams illustrating the experimental conditions used
88 (top) and representative live-cell confocal microscopy images of control (SCR) and ATGL-depleted
89 ($ATGL^{KD}$) MDA-MB-231 and HeLa cells treated with DGAT inhibitors during serum feeding (D) and
90 during serum starvation (E), without and with hGX $sPLA_2$ pre-treatment. LDs and nuclei were visualised
91 using BODIPY 493/503 and Hoechst 33342 staining and confocal microscopy. (**F**) Diagram illustrating
92 the experimental conditions (left) and graph showing DGAT inhibition (DGATi)-induced changes in PGE_2
93 production in serum-starved control (SCR) and ATGL-depleted ($ATGL^{KD}$) A549 cells, without and with
94 stimulation of LD biogenesis by hGX $sPLA_2$ pre-treatment. Neutral lipids were measured at the end of
95 starvation with Nile Red staining and flow cytometry. Lipid mediators were quantified by UPLC-MS-MS.
96 (F) PGE_2 levels were determined in cell supernatants as described in Methods. Data are means ±SEM
97 of three (A) or four (B, C) independent experiments. *, $P < 0.05$; **, $P < 0.01$; ***, $P < 0.001$ (two-way
98 ANOVA with Tukey (A), Sidak (B, C) or Bonferroni (F) adjustment). EPA, eicosapentaenoic acid; HEPE,
99 hydroxyeicosapentaenoic acid; AA, arachidonic acid; TXB_2, thromboxane B_2; HDHA,
100 hydroxydocosahexaenoic acid; HETE, hydroxyeicosatetraenoic acid; PGE_2, prostaglandin E_2; PGD_2,
101 prostaglandin D_2.

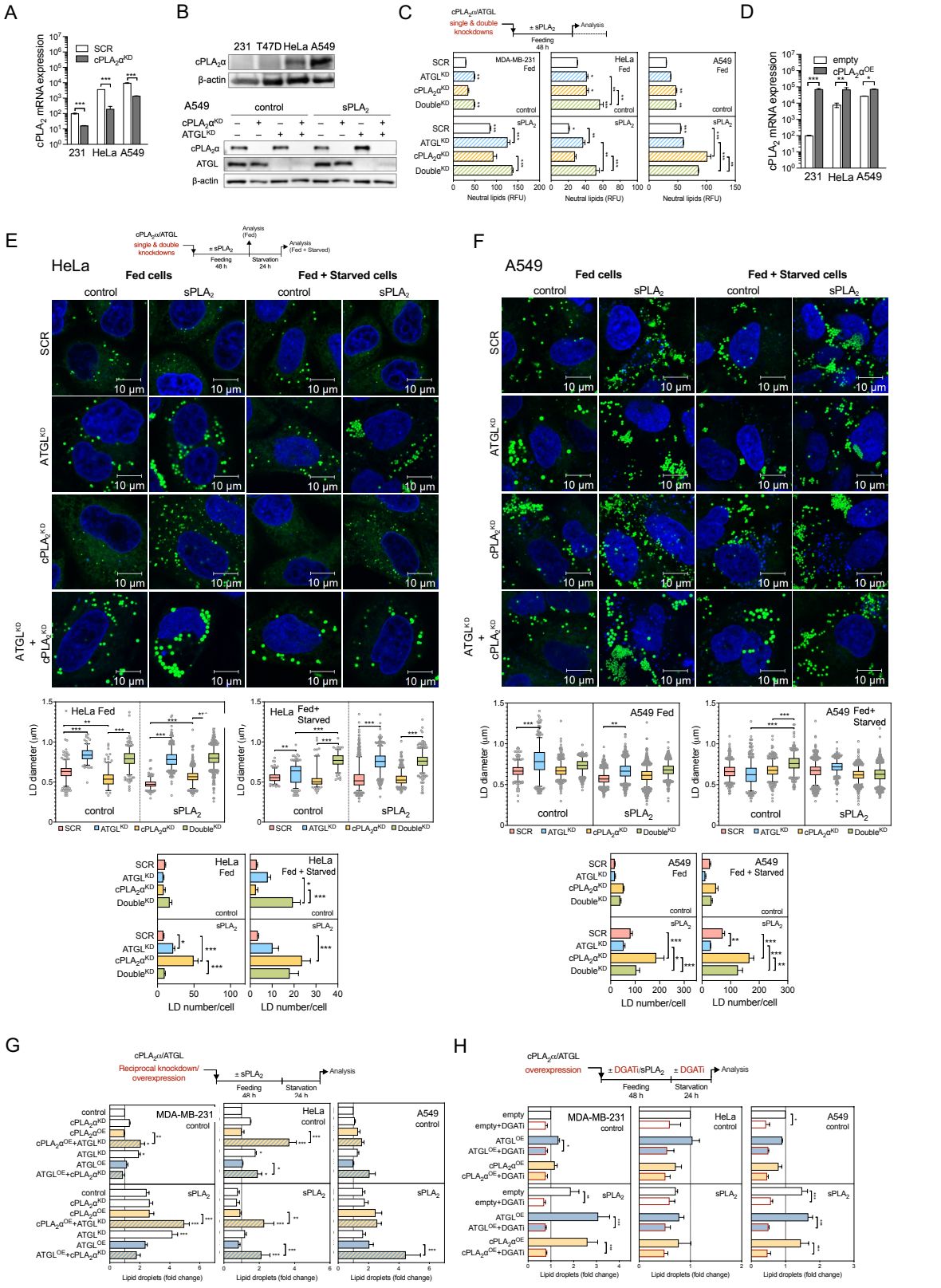

Supplementary Figure 5. cPLA$_2$α cooperates with ATGL in mediating LD-driven lipid mediator production. (**A**) Quantitative PCR analysis of cPLA$_2$α gene expression in control (SCR) and cPLA$_2$-knockdown (cPLA$_2$α^{KD}) cells grown for 48 h in complete medium and serum starved for 24 h. (**B**)

Representative western blots showing basal levels of $cPLA_2\alpha$ protein expression in the four cancer cell lines (top) and $cPLA_2\alpha$ and ATGL protein expression in single and double knockdown A549 cells, without and with hGX $sPLA_2$ pre-treatment (bottom). (**C**) Diagram illustrating the experimental conditions used (top), and changes in neutral lipid content in serum-fed cells induced by ATGL ($ATGL^{KD}$) and $cPLA_2\alpha$ ($cPLA_2\alpha^{KD}$) single and double ($Double^{KD}$) knockdowns, in comparison with control siRNA-treated cells (SCR), without and with stimulation of LD biogenesis by hGX $sPLA_2$ treatment. (**D**) Quantitative PCR analysis of $cPLA_2\alpha$ gene expression in control (empty) and $cPLA_2\alpha$-overexpressing ($cPLA_2\alpha^{OE}$) cells grown for 48 h in complete medium and serum starved for 24 h. (**E, F**) Diagram illustrating the experimental conditions used, representative live-cell confocal microscopy images and image analysis of LDs in ATGL ($ATGL^{KD}$) and $cPLA_2\alpha$ ($cPLA_2\alpha^{KD}$) single and double ($Double^{KD}$) knockdown HeLa and A549 cells, in comparison with non-targeting control siRNA-treated cells (SCR), without and with stimulation of LD biogenesis by hGX $sPLA_2$ pre-treatment. LDs were stained with BODIPY 493/503 (green) and nuclei with Hoechst 33342 (blue) and images analysed using ImageJ and the LD Counter Plugin. Box plots are showing changes in LD diameters and LD numbers per cell in serum-fed (Fed) and serum-starved (Starved) cells. Data are geometric means (diameter analysis) or means (number analysis) ±SEM (n >40 cells/sample) of two independent experiments. (**G**) Diagram illustrating the experimental conditions used (top), and neutral lipid levels in cells with reciprocal knockdown/overexpression of $cPLA_2\alpha$ and ATGL. Cells were reverse transfected with ATGL-targeting ($ATGL^{KD}$) and/or $cPLA_2\alpha$-targeting ($cPLA_2\alpha^{KD}$) siRNAs, then forward transfected with ATGL-encoding ($ATGL^{OE}$) and/or $cPLA_2\alpha$-encoding ($cPLA_2\alpha^{OE}$) plasmids, and/or pre-treated with hGX $sPLA_2$. In controls (control), non-targeting siRNA reverse transfections were combined with backbone ('empty') vector forward transfections. (**H**) Diagram illustrating the experimental conditions used (top), and DGAT inhibition (DGATi)-induced changes in neutral lipids in serum-starved control cells (empty) and in cells overexpressing ATGL ($ATGL^{OE}$) or $cPLA_2\alpha$ ($cPLA_2\alpha^{OE}$), without and with additional stimulation of LD biogenesis by hGX $sPLA_2$ pre-treatment. Neutral lipid content was quantified by Nile Red staining and flow cytometry. Data are means ±SEM of two (A, D; C, A549 cells) or at least three independent experiments. *, $P < 0.05$; **, $P < 0.01$; ***, $P < 0.001$ (unpaired t-tests (A, D); two-way ANOVA with Tukey (C, E–G) or Dunnet (H) adjustments; nested one-way ANOVA with Sidak adjustment (E, F)).

Supp. Fig. 6

A

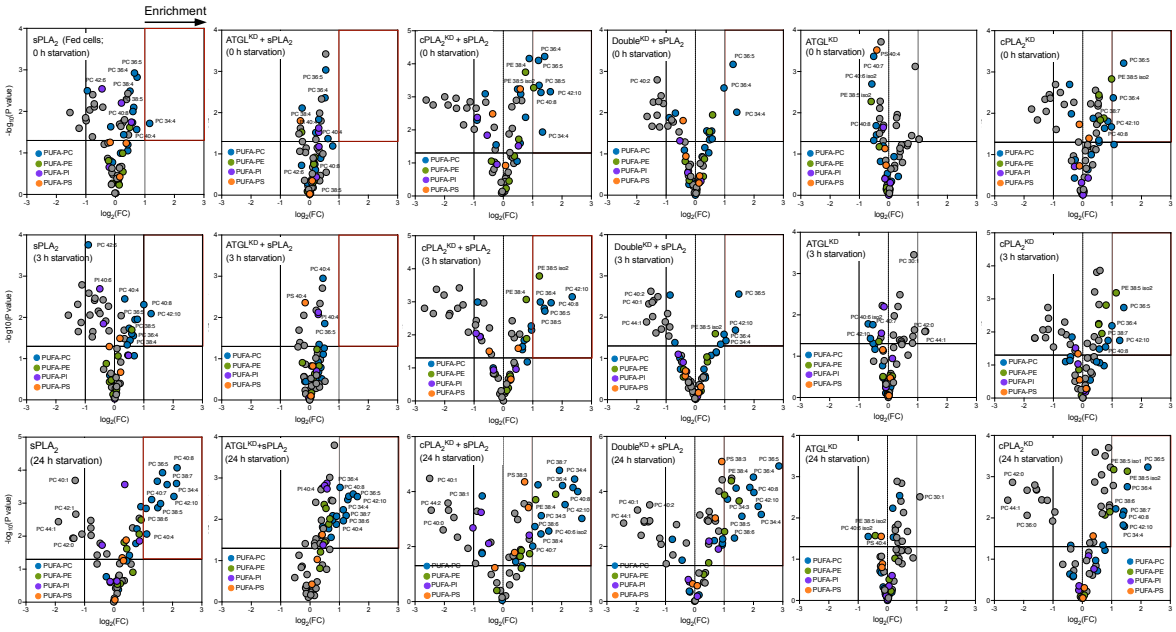

B

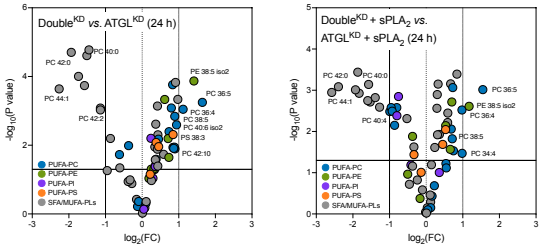

Supplementary Figure 6. Membrane phospholipid PUFA content is modulated by sPLA$_2$, cPLA$_2$α and ATGL. (**A, B**) Untargeted lipidomic analysis of phospholipids in MDA-MB-231 cells depleted of ATGL (ATGL^{KD}), cPLA$_2$α (cPLA$_2$α^{KD}) or both (Double^{KD}), without and with hGX sPLA$_2$ pre-treatment, and grown as shown in (B). Volcano plots show significant changes (–log$_{10}$(P value) >1.30) in individual lipids between each treatment condition *versus* control cells (unless otherwise indicated), and were prepared by log$_2$ fold-change (FC) data transformation and multiple t-test analysis (n=3 independent experiments). Phospholipids (PLs) containing saturated and mono-unsaturated acyl chains (SFA/MUFA-PLs with 0–2 double bonds) and those containing polyunsaturated FAs (PUFA-PLs with at least 3 double bonds) are colour-coded as indicated. PC, phosphatidylcholine; PE, phosphatidylethanolamine; PI, phosphatidylinositol, PS, phosphatidylserine.

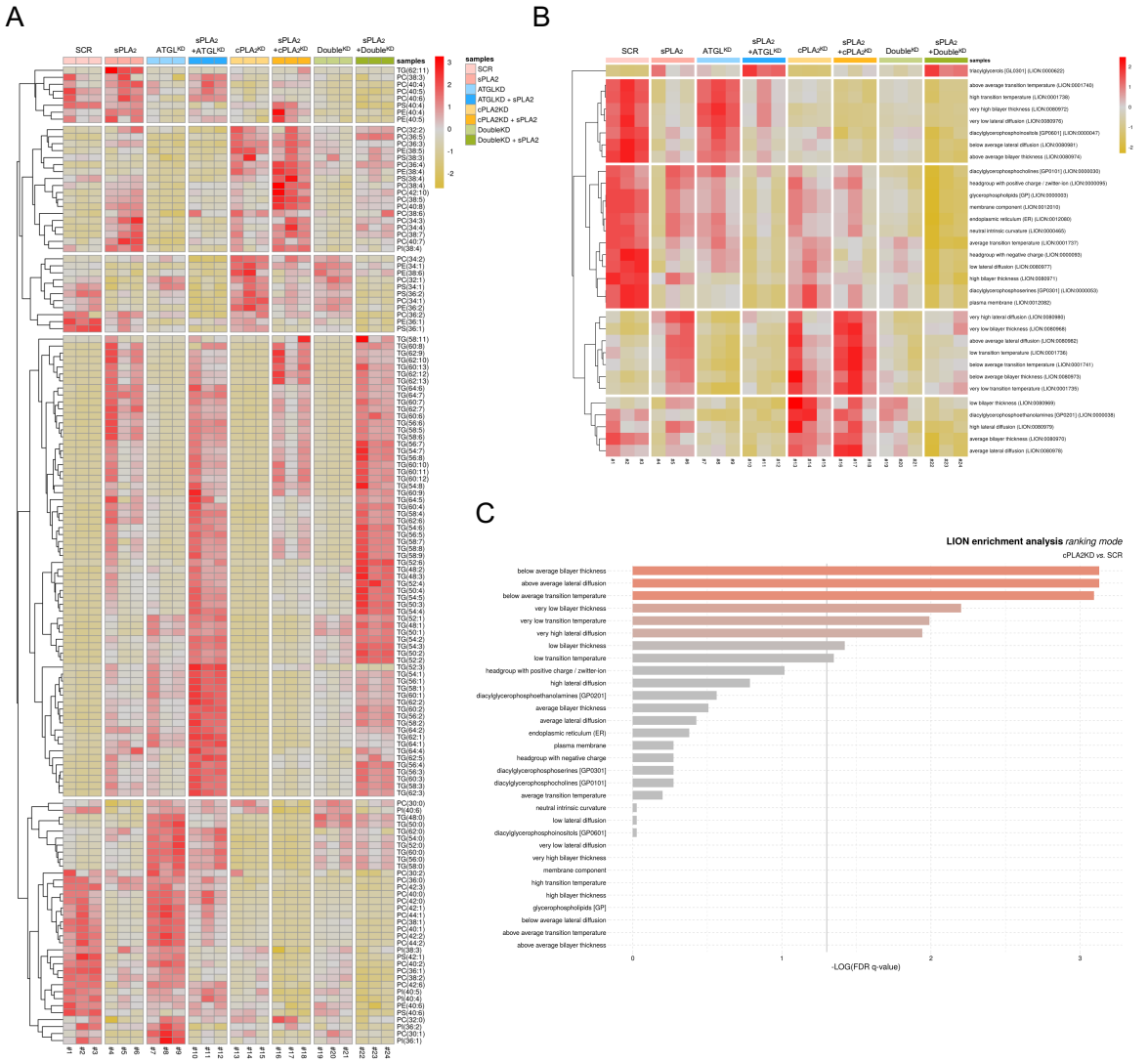

Supplementary Figure 7. LION-term enrichment analysis for significant changes in membrane properties induced by sPLA$_2$, cPLA$_2$α and ATGL. (**A**) Heat map of z-score scaled lipid levels of phospholipids and triglycerides in serum-starved MDA-MB-231 cells depleted of ATGL (ATGL^{KD}), cPLA$_2$α (cPLA$_2$α^{KD}) or both (Double^{KD}), without and with hGX sPLA$_2$ pre-treatment under serum-rich conditions. (**B, C**) LION-term enrichment analysis of the full data set (B) and pairwise comparisons of phospholipid data from cPLA$_2$α-depleted and control (SCR) cells (C) in ranking mode. The cut-off value of significant enrichments is indicated by the grey line (q <0.05). Data were analysed using three principal components, and lipids were clustered into five groups by hierarchical clustering (A, B). Bar colours are scaled according to the enrichment (−log q-values). FDR, false-discovery rate.

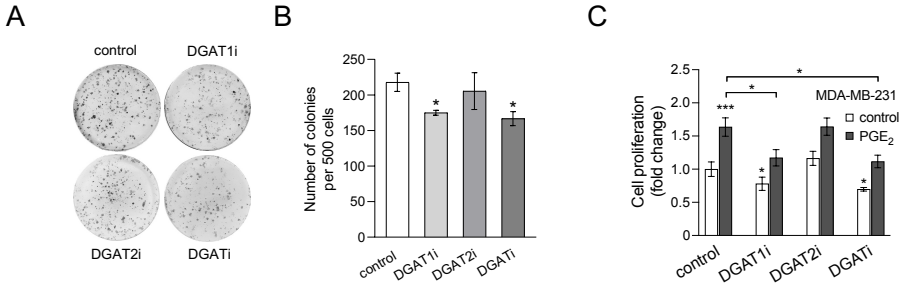

Supplementary Figure 8. Inhibition of DGAT1 reduces colony formation and PGE_2-induced proliferation in MDA-MB-231 cells. (**A, B**) Representative images (A) and graph (B) of DGAT inhibition-induced changes in colony formation of MDA-MB-231 cells treated grown in complete medium for nine days and treated with T863 (DGAT1i) and PF-06427878 (DGAT2i), or an equimolar mix of both DGAT inhibitors (DGATi). (**C**) Proliferation of MDA-MB-231 cells treated with 1 μM exogenous PGE_2 in the absence and presence of T863 (DGAT1i) and PF-06427878 (DGAT2i), or an equimolar mix of both DGAT inhibitors (DGATi). Data are means ±SEM of three independent experiments. *, $P < 0.05$; **, $P < 0.01$; ***, $P < 0.001$ (unpaired t-test (B); two-way ANOVA with Tukey (C) adjustment).